Received: 15 December 2024 | Revised: 16 May 2025 | Accepted: 28 May 2025

DOI: 10.1002/ar.70006

RESEARCH ARTICLE

The Anatomical Record | American Association for Anatomy | WILEY

Locomotor shifts, stylopod proportions, and the evolution of allometry in Synapsida

P. J. Bishop[1,2] | **S. E. Pierce**[1]

[1]Museum of Comparative Zoology and Department of Organismic and Evolutionary Biology, Harvard University, Cambridge, Massachusetts, USA

[2]Geosciences Program, Queensland Museum, Brisbane, Queensland, Australia

Correspondence
P. J. Bishop, Museum of Comparative Zoology and Department of Organismic and Evolutionary Biology, Harvard University, Cambridge, MA, USA.
Email: pbishop@fas.harvard.edu

Funding information
William F. Milton Fund, Harvard University; National Science Foundation, Grant/Award Numbers: DEB-1754459, EAR-2122115

Abstract

Locomotor evolution in synapsids involved numerous functional shifts associated with the transition from sprawled to erect limb postures on the line to therian mammals. Given that bone structure frequently reflects functional requirements, this study investigated evolutionary changes in synapsid humerus and femur proportions as a lens to evaluate functional shifts through time. A total of 936 bones were measured, representing 330 species across the full 320+ million years of synapsid history. This dataset was used to test whether transformations in stylopod proportions are consistent with inferred changes in bone loading mechanics, alignment of joint and muscle forces, muscular control of the shoulder and hip, and differential support of body weight by the fore- and hindlimbs. As variation in bone dimensions may also correlate with bone or body size, this study first developed a novel approach for calculating species-specific, size-corrected measures of bone proportions. By disentangling the effect of body size from functional signals recorded in bone geometry, this then enabled a node-to-node appraisal of how bone allometry itself evolved through time. Ancestral state reconstruction of size-corrected stylopod proportions reveals trends that broadly support many hypothesized shifts in locomotor biomechanics along the therian stem lineage. However, patterns of transformation are frequently complex, suggesting functional mosaicism, and stylopod proportions that typify therians as a whole are often not achieved until crown Theria itself. Several instances of temporary trend reversal are also inferred, particularly within non-mammalian cynodonts, indicating greater functional or ecological diversification in this group.

KEYWORDS

biomechanics, evolutionary allometry, locomotion, mammal, scaling, synapsid

1 | INTRODUCTION

The origin of mammals was a landmark series of events in the history of vertebrate evolution. Documented by an exceptionally rich fossil record spanning back over 320 Ma (Kemp, 1982, 2005, 2016), it involved profound transformation of almost every aspect of anatomy, physiology, and function. One such transformation was a major shift in stance and gait within their synapsid ancestors—from a plesiomorphic "sprawled" posture with the limbs held to the side of the body, to an "erect" (or parasagittal) posture typical of extant terrestrial therians. The sprawled-to-erect transition has been invoked as a key event underpinning the subsequent diversification of mammalian

locomotor behaviors, and more generally, their adaptive radiation into diverse ecologies (Dial et al., 2015; Kemp, 2005; Polly, 2007).

Unlike many other physiological systems, the evolution of locomotion is conducive to detailed scrutiny because a central component of locomotion, skeletal anatomy, is directly preserved in the fossil record. Moreover, locomotor evolution is amenable to investigation with a high level of quantitative rigor, through well-grounded principles and approaches in biomechanics (Bishop et al., 2021, and references cited therein). Thus, the study of synapsid locomotor anatomy, function, and its evolution has a long and rich history. In addition to documenting locomotor anatomy within and across higher taxonomic groups, most prior research has focused on understanding changes to musculature (see Bishop & Pierce, 2024a, 2024b and references cited therein) and joint anatomy (Bishop et al., 2023; Gambaryan & Kielan-Jaworowska, 1997; Hopson, 2015; Jenkins Jr & Parrington, 1976; Jenkins Jr., 1971b, 1973; Kemp, 1978, 1980a; Lai et al., 2018; Sereno, 2006), as well as their implications for posture, locomotor behavior, and its evolution (Boonstra, 1967; Brocklehurst et al., 2022; Colbert, 1948; De Oliveira & Schultz, 2016; Fröbisch, 2006; Guignard et al., 2019; Jenkins Jr., 1971b, 1973; Jones et al., 2021; Kemp, 1978, 1980a, 1980b, 1982; King, 1981, 1985; Lai et al., 2018; Ray & Chinsamy, 2003; Sullivan et al., 2013; Watson, 1917). From this body of research, it is clear that synapsid locomotor evolution was complex, with different parts of the body appearing to provide different signals as to when more typically mammalian locomotor patterns were acquired (Bishop & Pierce, 2024c; Jenkins Jr., 1971a; Jones et al., 2021; Kemp, 1982).

Beyond analyses focused on joint structure or musculature in non-mammalian synapsids, there has been comparatively little attention directed toward the functional significance of gross bony anatomy in and of itself. Quantitative characterization of fore- and hindlimb osteology has demonstrated that non-mammalian synapsids and early (Mesozoic) mammals had already achieved high ecomorphological disparity prior to the appearance of Theria (Brocklehurst et al., 2025; Chen & Wilson, 2015; Fröbisch & Reisz, 2009; Lungmus & Angielczyk, 2019, 2021). Anatomical and functional complexity in the synapsid vertebral column is also becoming better understood, highlighting a protracted and step-wise acquisition of therian-like traits over >100 Ma (Jones et al., 2018, 2020, 2021, 2024). Yet, the structural proportions of the limbs and their constituent bones, insofar as they relate to the mechanics of locomotion, have remained seldom studied (Blob, 2001, 2006; Brocklehurst et al., 2025; Romano, 2017; Rubidge et al., 1994). This stands in contrast to the well-known adaptability of bones and bone tissue to suit their functional requirements. In addition to being co-adapted with musculature and other soft tissues for effective execution of whole-limb function (e.g., Fujiwara & Hutchinson, 2012; Nakai & Fujiwara, 2023; Samuels et al., 2013; Sargis, 2002; Van Valkenburgh, 1987; Vogel, 2003), bone tissue is frequently tuned to the prevailing mechanical environment such that its structural arrangement can be highly reflective of the loads experienced in life (Barak, 2024; Bishop et al., 2018b; Carter & Beaupré, 2001; Currey, 2002; Frongia et al., 2018; Kivell, 2016; Martin et al., 1998; Pontzer et al., 2006). Analysis of bone structure can therefore provide important insights into locomotor biomechanics of extinct species (Alexander, 1989; Bishop et al., 2018a; Bishop et al., 2018b; Blob, 2001; Carrano, 1998; Christiansen, 1999a; Georgiou et al., 2020; Kivell, 2016; Lovejoy et al., 2002; Maidment et al., 2012; Pintore et al., 2022; Thomason, 1985).

As with many other locomotor transformations in history, the sprawled-to-erect transition in synapsids is expected to have entailed numerous shifts in biomechanics at different anatomical scales. In addition to obvious kinematic differences between sprawled and erect postures, experimental study of locomotion in extant tetrapods indicates contrasting strategies of muscular support and propulsion, with adductors and long-axis rotators dominating in sprawling postures, but abductors and retractors dominating in erect postures (Ashley-Ross,-1995; Gatesy, 1997; Goslow Jr et al., 1981; Jenkins Jr & Goslow Jr., 1983; Jenkins Jr & Weijs, 1979; Reilly, 1995). Hence, major changes in muscle function likely occurred throughout synapsid history, consistent with major anatomical reorganization as deduced from the fossil record (Bishop & Pierce, 2024a, 2024b). Not surprisingly, differences in limb kinematics and muscle function engender marked differences in bone loading mechanics between sprawled and erect postures, as documented through in vivo experimental studies. Whereas the bones of sprawling taxa are loaded primarily in torsion (Blob et al., 2014; Blob & Biewener, 1999; Butcher et al., 2008; Sheffield et al., 2011; Sheffield & Blob, 2011; Young et al., 2017), those of erect therians are mostly loaded by bending and axial compression (Aamodt et al., 1997; Biewener, 1991; Copploe et al., 2015; Szivek et al., 1992), although torsional loading may still be significant in taxa that use more crouched postures (Butcher et al., 2011; Keller & Spengler, 1989). These comparisons suggest that synapsids evolved from a torsion-dominant to bending-dominant loading regime over their history (see also Blob, 2001, 2006).

Synapsids also exhibited a progressive redistribution of body mass across their history. Whereas basal

members (i.e., Permo-Carboniferous "pelycosaurs") were typified by small heads and long tails (Romer & Price, 1940), superficially resembling lizards or crocodylians in overall form, extant terrestrial therians are typified by large heads and small tails. Reflecting these contrasts, the whole-body center of mass in extant lizards and crocodylians is positioned closer to the pelvis (Allen et al., 2009; Macaulay et al., 2023), whereas that of most therian mammals lies closer to the pectoral girdle (Alexander, 2006; Buchner et al., 1997; Coatham et al., 2021). It is therefore reasonable to expect that an anterior shift of the center of mass occurred along at least some part of the therian stem lineage, although evolutionary trends are yet to be explicitly quantified (but see Wright et al., 2024). In attaining a more anteriorly positioned center of mass, the forelimb would progressively acquire an increasing role in weight support and body movement compared to the hindlimbs (cf. Cieri et al., 2021; Demes et al., 1994; Pandy et al., 1988; Ren et al., 2010; Willey et al., 2004; Witte et al., 2004), and this may have impacted bone loading mechanics.

Given the multitude of mechanical factors that presumably changed throughout synapsid locomotor evolution, and considering the great adaptability of bone to meeting its functional requirements, it stands to reason that careful analysis of fossil osteology can provide insights on these factors. The present study sought to investigate evolutionary changes in synapsid locomotor biomechanics through the lens of stylopod (humerus and femur) gross proportions. In addition to being central to fore- and hindlimb function, the humerus and femur are among the most frequently preserved postcranial elements in the synapsid fossil record, and their larger size and more robust construction mean that they tend to preserve better than other postcranial elements. A very large sample size can therefore be assembled (Brocklehurst et al., 2025; Lungmus & Angielczyk, 2019), and in the present study, almost 600 individual fossil bones were able to be measured. With such a comprehensive sample of synapsid history, the present study aimed to test the overarching hypothesis that evolutionary transformation in humeral and femoral proportions is consistent with:

1. A change in bone loading regime, from torsion- to bending-dominant;
2. Realignment of the bones to function in a plane more parallel to the body, and the attendant realignment of joint and muscle forces;
3. Changes in the efficacy of major muscles crossing the shoulder and hip joints; and
4. The forelimb becoming more prominent in body weight support.

If stylopod proportions are indeed consistent with these presumed functional shifts, observed temporal patterns in proportions can complement and enrich interpretations developed at broader anatomical scales. However, since changes in absolute size can exert a strong influence on internal and external anatomical dimensions, both within and across species (Carrier, 1983; Carrier & Leon, 1990; Christiansen, 1999b; Doube et al., 2012, 2018; Galilei, 1638; Schmidt-Nielsen, 1985; Swartz & Biewener, 1992; Taylor & Thomas, 2014), exploration of stylopod proportions must first be capable of differentiating the effects of body size from those of functional demands. To that end, this study also proposes a new quantitative framework for disentangling these effects on bony morphology throughout evolution, which facilitates a fine-grained view of the evolution of allometry across major functional transitions. The generality of this framework enables its potential application to a wide range of questions involving organismal allometry across broad taxonomic and temporal scales.

2 | MATERIALS AND METHODS

2.1 | Taxon and specimen sampling

Humeri and femora were sampled from across the entire history of Synapsida, in addition to a selection of stem amniotes serving as an outgroup (Figure 1; see also Figures S1–S3). A further three well-preserved and historically important fossil synapsid specimens—two gorgonopsians (Boonstra, 1934; von Huene, 1950) and a dicynodont (Govender, 2008)—were also included; their precise alpha taxonomy remains unresolved, but their relationships with respect to the other taxa investigated here are generally understood. To help infer the ancestral therian condition as a point of reference, a large sample of extant therians and one stem marsupial were measured. Two extant monotreme species were also included to help refine inferences for the crown mammal node. In total, 330 species-level operational taxonomic units (OTUs) were sampled: seven stem amniotes, 33 non-therapsid synapsids ("pelycosaurs"), 72 non-cynodont therapsids ("therapsids"), 36 non-mammalian cynodonts ("cynodonts"), 11 non-therian mammals, and 171 therians. Wherever possible, sampling focused on large, well-preserved specimens that (for fossils) appeared to have undergone minimal taphonomic deformation. Additionally, data were preferentially collected from specimens in which both humerus and femur could be confidently ascribed to a single individual.

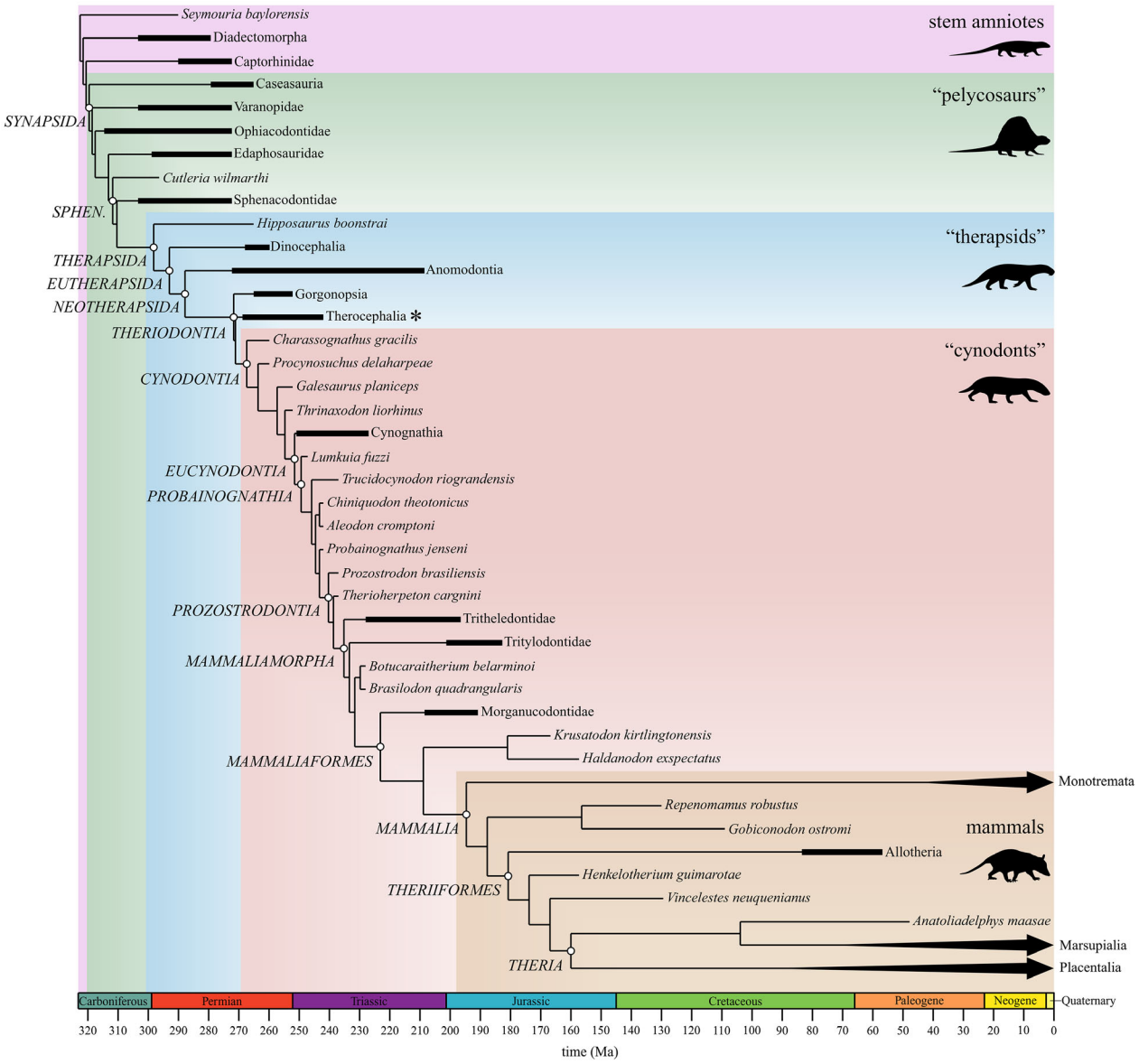

FIGURE 1 Simplified representation of the phylogenetic and temporal relationships of the taxa studied, with major nodes and paraphyletic grades of organization indicated. See Figures S1–S3 for fully resolved, time-calibrated phylogenies for each taxon. The temporal range of taxa sampled for each clade is indicated by black bars. "Sphen." denotes Sphenacodontia; asterisk indicates that Therocephalia may be paraphyletic with respect to Cynodontia (see Figure S3).

Owing to specimen incompleteness or inaccessibility, many more fossil specimens were measured than species (936 bones belonging to 647 specimens; Supporting Information S2); rarely was a single specimen able to provide all the desired measurements for a given species. Thus, to maximize the utility of the data collected, each species was represented in the analyses by a single "focal specimen" for which missing data was composited from measurements made for other available specimens pertaining to the same taxon. As some analyses involved diaphyseal metrics from both humerus and femur (see below), the largest available individual comprising both humerus and femur was prioritized in determining the focal specimen for a given species. Hence, the focal individual may not necessarily be the largest individual that was able to be measured. If no individual with both humerus and femur was sampled, then the largest individual measured was generally selected to serve as the focal specimen, unless another was particularly well measured (i.e., almost all measurements for a given bone could be derived from a single specimen). Which specimen served as the focal specimen in each species is indicated in Supporting Information S2, and the final dataset is presented in Supporting Information S3.

In attempting to fill in missing data, if only one other specimen of a given species was available to estimate missing measurements, then its measurement was linearly scaled to the focal individual by virtue of bone length. However, if two or more specimens were available, then their measurements were regressed against bone length (using a linear relationship on logarithmic coordinates), which was used to estimate the required measurement of the focal individual by virtue of bone length. Lastly, although multiple species of *Lystrosaurus* were sampled over the course of the study, due to various constraints exceedingly few specimens assignable to the genus were assignable at the species level, and those specimens that could be designated at the species level comprised only a humerus or femur. Thus, a composite "*Lystrosaurus* spp." OTU was created instead. After filling in missing data for focal specimens as much as possible, overall completeness of the humerus dataset was 85.6%, and that of the femur dataset was 84.5%.

2.2 | Raw measurements

Thirteen linear measurements were made for the humerus, while 11 linear measurements were made for the femur, in addition to one angular measurement (Figure 2). All measurements characterize external morphology only. As this study fundamentally sought to investigate how mechanics, rather than anatomy itself, changed on the line to mammals, measurements focused on aspects that have clear mechanical relevance to bone loading and locomotor function. Anatomical and functional terminology employed here follows that outlined previously (Bishop & Pierce, 2024a, 2024b; Brocklehurst et al., 2022).

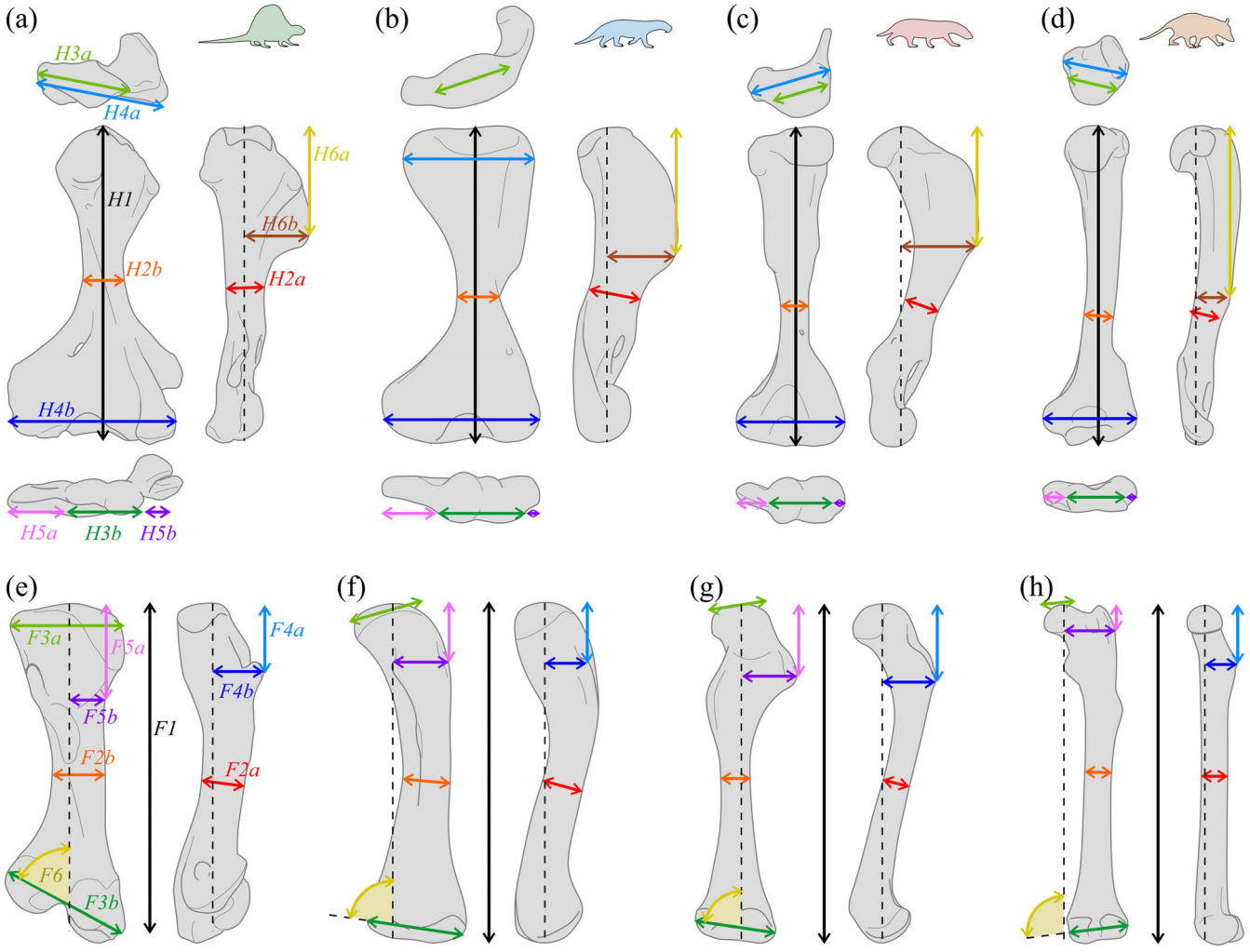

FIGURE 2 Illustration of the measurements made on the humerus (a–d) and femur (e–h), shown for representative morphologies of "pelycosaurs" (a, e), non-cynodont therapsids (b, f), non-mammalian cynodonts (c, g) and mammals (d, h). Humeri are illustrated in proximal, dorsal, anterior and distal views; femora are illustrated in ventral and medial views. Note that measurements F4a and F4b could not be measured for many dicynodonts, as the internal trochanter is typically not expressed in these taxa (Bishop and Pierce, 2024b).

2.2.1 | H1 (humerus) and F1 (femur)

Proximodistal length, taken as the maximal distance from the proximal to distal articular surfaces, measured parallel to the long-axis of the bone, which is typically indicated by the diaphysis. Overall bone length dictates the relative sizes of muscle and joint force in- or out-levers, and also influences the magnitude of bending or torsional stresses experienced during use (Blob, 2001; Currey, 2002). Additionally, bone length is used here as the basis for accounting for differences in absolute bone size, as described below.

2.2.2 | H2a–d (humerus) and F2a–d (femur)

Diameters of the diaphysis, measured in a single cross-sectional plane through the narrowest point of the shaft, which is not necessarily mid-way along the length of the bone. Measure (a) is taken in the dorsoventral (humerus) or anteroposterior (femur) direction, and measure (b) is taken in the anteroposterior (humerus) or mediolateral (femur) direction, perpendicular to (a). More precisely, in the humerus, H2a is measured perpendicular to the axis in which the distal end of the bone is most expanded, which does not necessarily correspond to the axis joining radial and ulnar condyles. In the femur, F2a is measured perpendicular to the plane containing the bone long-axis and the axis of the femoral condyles. Two additional measurements were made for both the humerus and femur, capturing the maximum (H2c, F2c) and minimum (H2d, F2d) diameters, irrespective of their orientation with respect to the diaphysis. Diaphyseal diameter is strongly tied to cross-sectional area and second and polar moments of area, which collectively contribute to a bone's efficacy at resisting compression, bending, and torsional loading (Biewener, 1992; Currey, 2002; Wainwright et al., 1976). For example, bones subject to torsion-dominant loading may have a greater polar moment of area compared to those not subject to strong torsional loads, for a given cross-sectional area (Doube et al., 2012), which is what would be expected from first principles (Beer et al., 2012; Main et al., 2021). The present study targets the narrowest point in the diaphysis as this will likely correspond to where compression, bending, and torsional resistance of the bone are lowest, and thus perhaps the region most relevant to tissue-imposed limits of locomotor loading. Such a presumption must be made cautiously, however, as it is seldom verified in empirical studies, and indeed maximal limb bone strain may occur elsewhere due to variation in cortical bone thickness and local muscle-induced loading (Biewener et al., 1986; Brassey et al., 2013).

2.2.3 | H3a–b (humerus) and F3a–b (femur)

Maximum width of proximal (a) and distal (b) articular surfaces. Proximally, this is measured parallel to the long axis of the articular surface, excluding any adjacent tuberosities or trochanters. In the distal humerus, H3b is measured parallel to the "distal bone axis" outlined above. In the distal femur, F3b is measured parallel to the axis of the femoral condyles, approximated by an imaginary cylinder fit to the articular surfaces, thus describing the width of the bone approximately perpendicular to the primary axis of movement at the knee. The width of an articular surface contributes to the capacity for withstanding large external joint moments, either by active or passive soft tissue forces, and hence can contribute to joint stability (Currey, 2002). This is especially pertinent for off-axis moments that the muscular system is poorly suited to controlling, such as abduction–adduction of the knee. Excessively broad articular surfaces may also involve a compromise of restricted joint mobility in certain directions (e.g., Brocklehurst et al., 2022; Currey, 2002; Regnault et al., 2021), or suboptimal lubrication and loading of articular cartilage, especially in fast motions (Marquez-Florez et al., 2024).

Measures H4a–H6b collectively describe the extent to which certain key forelimb muscles have leverage at the shoulder and elbow joints, and thus capture aspects related to joint movement and stability.

2.2.4 | H4a–b

Maximum width of the proximal (a) and distal (b) epiphyses of the humerus. Proximally, this is measured parallel to the long-axis of the humeral head as a whole, including any adjacent tuberosities; this includes the hypothesized insertion of the supracoracoideus, denoted by an angle if not an explicit scar of attachment (Bishop & Pierce, 2024a). Distally, this is measured parallel to the distal bone axis and includes the entepicondyle and ectepicondyle (but not the supinator process in the case of "pelycosaurs"). As with the articular surfaces, broader epiphyses can contribute to a greater capacity for joint moment control.

2.2.5 | H5a–b

Maximum width of the (a) entepicondyle and (b) ectepicondyle of the humerus. H5a is measured from the apex of the entepicondyle to the posterior edge of the ulnar condyle articular surface, and H5b is measured from the apex of the ectepicondyle to the anterior edge of

the radial capitulum articular surface. Both measurements are made parallel to the distal bone axis, and hence H3b + H5a + H5b = H4b. By describing the "overhang" of the epicondyles, H5a and H5b capture the leverage of the forearm flexor (H5a) and extensor (H5b) muscles with respect to the elbow, particularly in terms of abduction–adduction. A well-developed entepicondyle has previously been correlated with adaptation for sprawled forelimb postures (Fujiwara & Hutchinson, 2012; Romer, 1922), as such poses are expected to incur large off-axis adduction (radial deviation) joint moments at the elbow that can be partially countered by forearm flexor muscles.

2.2.6 | H6a–b

Distal extent (a) and depth (b) of the deltopectoral crest of the humerus. H6a is measured from the proximal end of the humerus to the distal apex of the crest, parallel to the bone's long axis. H6b is measured from the distal apex of the crest to an imaginary inter-articular axis running between the centers of the articular surfaces (Figure 2a–d, dashed line); it is measured perpendicular to this axis, irrespective of the anatomical orientation of this perpendicular. These measurements primarily capture the positioning of the insertion of the pectoralis musculature and its capacity for effecting shoulder depression, which is relevant to the stance phase in both sprawled and erect forelimb postures (although for differing reasons; see Brocklehurst et al., 2022).

2.2.7 | F4a–b

Distal positioning (a) and depth (b) of the "anteroventral trochanter" of the femur, corresponding to the internal trochanter of herpetology and the lesser trochanter of mammalogy (Bishop & Pierce, 2024b). F4a is measured from the proximal end of the femur to the apex of the trochanter, parallel to the bone's long axis. F4b is measured from the apex of the crest to an imaginary axis running parallel to the femoral long-axis and passing through (projecting from) the center of the femoral head, which may therefore not pass through the middle of the distal condyles (Figure 2e–h, dashed line); it is measured perpendicular to this axis, irrespective of the anatomical orientation of this perpendicular. These measurements capture the positioning of the puboischiofemoralis externus (PIFE) and, subsequently in more derived synapsids, the puboischiofemoralis internus (PIFI) musculature, which have different origins and functions in extant tetrapods (Bishop & Pierce, 2024b).

2.2.8 | F5a–b

Distal positioning (a) and depth (b) of the insertion of the iliofemoralis (IF) musculature or its derivative, the mammalian gluteals, on the femur. In therapsids the IF insertion is demarcated by the greater trochanter, whereas no bony prominence is present in "pelycosaurs" or stem amniotes. Nevertheless, faint scarring in some specimens indicates that the muscle's general locus of attachment was centered at the point of inflection of the lateral margin of the femur in these animals (Figure 2e; Bishop & Pierce, 2024b). Both measurements are made in the same fashion as H4a–b, with the lateralmost part of the insertion being the point of reference. In some taxa, especially placentals, this does not necessarily correspond to the "apex" of the muscle attachment, wherein the greater trochanter develops a marked proximal projection. In describing the positioning of the IF, these measurements capture the efficacy of this key hip muscle in hip abduction.

2.2.9 | F6

The angle between the axis of the femoral condyles and the long axis of the bone, measured in posterior view on the medial side of the long axis. Distinctly beveled femoral condyles, with the lateral condyle more distally positioned than the medial (acute F6 in the convention used here), are characteristic of extant sprawling tetrapods, wherein skewed joint axes help maintain the pes in a more anteriorly facing orientation during locomotion (Rewcastle, 1980, 1983). Such beveling is prominent in stem amniotes and "pelycosaurs," consistent with their interpretation as habitual sprawlers (Romer & Price, 1940; Sumida, 1997), but in extant therians is minimally developed or even slightly reversed (as in humans).

Wherever possible, measurements were made directly on physical specimens accessioned in publicly accessible museum collections (Supporting Information S2), using digital calipers (0.1 mm resolution) for measurements 150 mm or less, or flexible tape (1 mm resolution) for measurements greater than 150 mm. Measurement F6 was made with a transparent plastic protractor, rounded to the nearest 5°. In a very small number of specimens, measurements were made on digital models of the bones (using Rhinoceros 4.0; McNeel, USA) that had been generated via laser surface scanning, photogrammetry, or x-ray computed tomographic scanning; see Supporting Information S2 for full details.

2.3 | Derived metrics

Several additional metrics were derived from the above raw measurements to gain additional insight into various biomechanical aspects related to locomotion.

2.3.1 | Diaphyseal asymmetry

Basic beam theory would indicate that diaphyses with a more circular cross-section are more resistant to torsional loads than less circular diaphyses with the same cross-sectional area. Conversely, more elliptical diaphyses are better resistant to bending moments in the plane containing the major axis of the ellipse (Beer et al., 2012; Wainwright et al., 1976). If limb bone loading shifted from torsion-dominant to bending- or compression-dominant across the course of synapsid history, the null expectation would be that humerus and femur diaphyseal asymmetry (HDA and FDA, respectively) increased on the line to mammals. Indeed, in a previous survey of non-mammalian synapsid femora, Blob (2001) observed a progressive increase in FDA from basal synapsids to theriodont therapsids, providing some support for this expectation (although FDA was reduced in non-mammalian cynodonts). However, comparison between a large sample of extant sprawling saurians (Blob, 2000) and erect carnivorans (Bertram & Biewener, 1990) reveals little difference in femoral diaphyseal asymmetry (Figure S4). The relationship between diaphyseal asymmetry and bone loading or locomotor posture, or how it evolved over time, is therefore more complex than first principles may suggest. To provide a comprehensive assessment of this issue, diaphyseal asymmetry in both the humerus and femur was computed here as the ratio of maximal to minimal diameters,

$$\mathrm{HDA} = \frac{\mathrm{H2c}}{\mathrm{H2d}}, \tag{1a}$$

$$\mathrm{FDA} = \frac{\mathrm{F2c}}{\mathrm{F2d}}. \tag{1b}$$

2.3.2 | Relative diaphyseal robustness

Tail reduction and head enlargement would probably be associated with an anterior shift in the whole-body center of mass in synapsids on the line to therian mammals. It would therefore be expected that the forelimbs would acquire a progressively greater role in weight support compared to the hindlimbs, irrespective of changes in limb posture. Bearing relatively increased loads, the humerus in turn ought to become progressively more robust compared to the femur in progressively more crownward synapsid taxa. One approach to evaluating relative diaphyseal robustness (RDR) is to compute the ratio of the diaphyseal circumferences of the humerus and femur. Given that the diaphyses may have markedly different maximum and minimum diameters, circumferences are better estimated by assuming an elliptical cross-section to the diaphysis, rather than a circular one. Thus, RDR is computed as

$$\mathrm{RDR} = \frac{\pi \cdot \left(3 \cdot \left(\frac{\mathrm{H2c}}{2} + \frac{\mathrm{H2d}}{2}\right) - \sqrt{\left(3 \cdot \frac{\mathrm{H2c}}{2} + \frac{\mathrm{H2d}}{2}\right) \cdot \left(\frac{\mathrm{H2c}}{2} + 3 \cdot \frac{\mathrm{H2d}}{2}\right)}\right)}{\pi \cdot \left(3 \cdot \left(\frac{\mathrm{F2c}}{2} + \frac{\mathrm{F2d}}{2}\right) - \sqrt{\left(3 \cdot \frac{\mathrm{F2c}}{2} + \frac{\mathrm{F2d}}{2}\right) \cdot \left(\frac{\mathrm{F2c}}{2} + 3 \cdot \frac{\mathrm{F2d}}{2}\right)}\right)}, \tag{2}$$

following Ramanujan (1914). Trends in RDR can provide a first approximation of how whole-body center of mass location may have shifted throughout synapsid evolution, in lieu of an explicit quantitative assessment (e.g., Bates et al., 2016; Macaulay et al., 2023; Wright et al., 2024). For maximum rigor, RDR was only computed for taxa where both humerus and femur were available for the focal specimen.

2.3.3 | Humeral tuberosities

One of the more conspicuous aspects of forelimb muscle evolution in synapsids was the dorsal migration and differentiation of the supracoracoideus mass to form the infra- and supraspinatus, in addition to the clavicular deltoid and part of the pectoralis major (Smith-Paredes et al., 2022). Abundant osteological evidence of this transformation is recorded in non-mammalian synapsid fossils (Bishop & Pierce, 2024a). Among other things, this includes the appearance of a greater tuberosity in cynodonts (insertion of the infra- and supraspinatus), in addition to a lesser tuberosity (insertion of the subscapularis, and subcoracoideus if it existed) that has persisted since stem amniotes. Potentially, the degree of development of these tuberosities may be indicative of the relative importance or function of their attaching muscles to actuating or stabilizing the shoulder joint. To assess whether any major trends exist, tuberosity development was quantified as

$$\mathrm{HT} = \frac{\mathrm{H4a}}{\mathrm{H3a}}. \tag{3}$$

By expressing how much beyond the dimensions of the shoulder joint these tuberosities project, HT gives

some measure of the leverage of the muscles that attach(ed) here.

2.3.4 | Femoral trochanters

In the hindlimb, substantial reorganization of the hip musculature occurred on the line to mammals, including the expansion and differentiation of the IF mass dorsally, reduction and posterior migration of the PIFE mass ventrally, and progressive dorsal migration of the (initially ventral) PIFI mass. The complex history of these transformations is also recorded by abundant osteological evidence, involving two eminences, the greater and anteroventral trochanters (Bishop & Pierce, 2024b; Jenkins Jr., 1971b). Whereas the greater trochanter consistently remained the site of insertion of the IF mass, the anteroventral trochanter initially served as the attachment for the PIFE ("internal trochanter"), which was subsequently replaced by the PIFI in early eucynodonts ("lesser trochanter"). All three muscle groups play important roles during locomotion in extant sprawling and erect tetrapods as key hip abductors, adductors, protractors, or retractors (e.g., Dick & Clemente, 2016; Goslow Jr et al., 1981; Nicolopoulos-Stournaras & Iles, 1984; Pierce et al., 2020; Reilly, 1995), and so tracking the positioning of the two trochanters may provide insight into the muscles' functional evolution on the line to mammals. This was assessed by comparing the proximodistal positioning of the trochanters' apices:

$$\mathrm{FT} = \frac{\mathrm{F5a}}{\mathrm{F4a}}. \tag{4}$$

skull (Brocklehurst, 2019; Huttenlocker, 2014), lower jaw (Hellert et al., 2023), vertebral centra (Brocklehurst & Brink, 2017; Romer & Price, 1940), and femur (Huttenlocker et al., 2021; Singh et al., 2024), as well as a combination of measures from the cranium and postcranium (Filippini et al., 2022; Kaiuca et al., 2024). The generality of these approaches to interpreting body size evolution across Synapsida as a whole remains to be established, as individual skeletal dimensions may vary substantially across phylogenetically and ecologically diverse groups. Among extant terrestrial amniotes, body mass has been shown to correlate with stylopod diaphyseal dimensions, such as circumferences (Campione & Evans, 2012, and references cited therein), reflecting these bones' direct involvement in body weight support. The data collected in the present study therefore offer the opportunity for an updated evaluation of body mass evolution across synapsids. However, a growing body of evidence suggests that empirical equations derived from extant taxa may give poor estimates for anatomically or posturally dissimilar extinct taxa, including non-mammalian synapsids (Bates et al., 2015; Brassey et al., 2015; Richards et al., 2019; Romano et al., 2021; Romano & Manucci, 2021; Romano & Rubidge, 2021; Wright et al., 2024). To that end, this study uses diaphyseal dimensions as a proxy for body mass, but stops short of estimating body mass itself. Again assuming an approximately elliptical cross-section of the diaphyses, maximum and minimum diameters can be used to estimate the sum of humeral and femoral diaphyseal circumferences as a proxy for body size, as

$$\mathrm{BS} \approx \frac{\pi \cdot \left(3 \cdot \left(\frac{\mathrm{H2c}}{2} + \frac{\mathrm{H2d}}{2}\right) - \sqrt{\left(3 \cdot \frac{\mathrm{H2c}}{2} + \frac{\mathrm{H2d}}{2}\right) \cdot \left(\frac{\mathrm{H2c}}{2} + 3 \cdot \frac{\mathrm{H2d}}{2}\right)}\right) + \pi \cdot \left(3 \cdot \left(\frac{\mathrm{F2c}}{2} + \frac{\mathrm{F2d}}{2}\right) - \sqrt{\left(3 \cdot \frac{\mathrm{F2c}}{2} + \frac{\mathrm{F2d}}{2}\right) \cdot \left(\frac{\mathrm{F2c}}{2} + 3 \cdot \frac{\mathrm{F2d}}{2}\right)}\right)}{}. \tag{5}$$

2.3.5 | Body size

Although it is clear that body size varied considerably throughout synapsid history (Kemp, 1982, 2016), rigorous assessments of body size evolution remain in their infancy. Prior analyses have used both direct and indirect estimates of body size in non-mammalian synapsids or select subgroups, based on dimensions of the

Although this metric cannot be uniformly related to body mass, it is reasonable to suspect that higher values in one taxon relative to closely related (i.e., anatomically and posturally similar) taxa genuinely indicate higher body masses. This comparative framework can also be applied to adjacent internal nodes in the synapsid phylogeny, thus enabling a semi-quantitative evaluation of phyletic increases or decreases in body size. To reduce the

effects of very large body size having a skewing effect on downstream results (Benson et al., 2022), the base-10 logarithm of this metric was first taken prior to subsequent analysis. Hence, results for body size should be viewed as a proxy for logarithmically transformed body mass, not body mass itself.

2.4 | Size-independent quantification of bone proportions

At the level of the organism—the level at which selection acts—biomechanical function is most strongly dictated by gross bone dimensions, since these determine muscle–joint mechanical advantage, the magnitude of applied bending and torsional moments, and the ability of the bone to withstand applied loads. These dimensions will typically increase with increases in absolute size of the bone. The standard approach to making sense of variation in any continuously varying trait (such as bone dimension) across a sample of different-sized species is to regress the trait of interest against a measure of size, such as bone length. This well-established exercise in interspecific scaling (Schmidt-Nielsen, 1985; Swartz & Biewener, 1992; Taylor & Thomas, 2014) clarifies the covariation between a given trait and size across a static sample of species, and how this relationship compares to that in a separate, static sample. However, such an approach has three important limitations that reduce its utility for drawing evolutionary inferences.

Firstly, a scaling relationship is a fictitious abstraction that only exists as an emergent property of multiple species considered together (Kozłowski & Wiener, 1997); the phenotype of a given species is only interpretable in relation to some external point of reference (even though traits will evolve in each species independent of other species). As a consequence, the recovered scaling relationship can markedly differ depending on the scope of the included species, such as the taxonomic resolution of the group to which the regression is fit (Bertram & Biewener, 1990; Chan, 2016; Christiansen, 1999b; Labonte et al., 2016; Spence, 2009; Venditti et al., 2024). Secondly, deriving scaling relationships in multiple groups precludes assessment of how a trait changes from one species to another, that is, how it evolves. Despite describing continuously varying traits, the creation of group-level scaling relationships renders the only possible evolutionary pattern as one of a discrete step change. Furthermore, the taxa within each group are variously related to taxa in the other group(s) to differing degrees, rendering any evolutionary interpretation nonsensical, as trait evolution proceeds from one species to another, not one group to another. Characterizing scaling

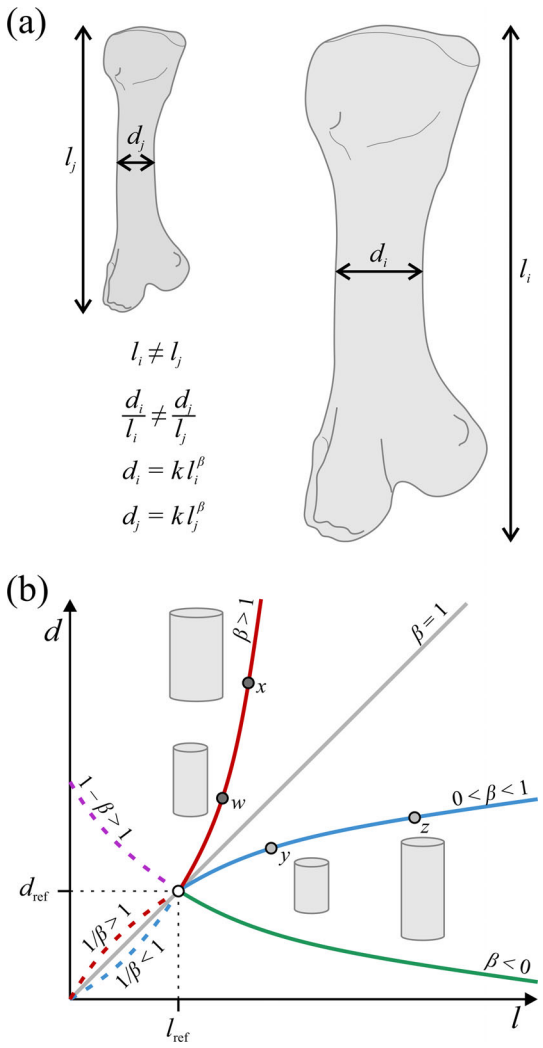

FIGURE 3 Deriving a size-independent measure of bone robusticity. (a) Hypothetical bones of two different species, with different absolute and relative dimensions that satisfy a common allometric scaling relationship described by k and β. (b) Graphical manifestation of the meaning of different values of β, calculated with respect to a reference bone of length l_{ref} and other dimension d_{ref}. Species w and x plot on the same allometric curve and are thus equally robust for their size; the same is true for species y and z. At lengths less than l_{ref}, the magnitude of β needs to be interpreted differently to maintain consistency with respect to greater or lesser robusticity; this complexity can be avoided by choosing a suitably small reference bone (i.e., small l_{ref}).

relationships across groups therefore cannot elucidate how the scaling relationship itself has changed in an evolutionary sense (cf. Venditti et al., 2024), even if one group is paraphyletic with respect to another (Chan, 2016; Gatesy, 1991; Maidment et al., 2012; McPhee et al., 2018). Lastly, it has long been known that covariation between traits and size can be non-isometric (Galilei, 1638). While differences in bone proportions from one species to another may be indicative of

differences in function, they may also be linked to differences in absolute size. The problem is thus posed of how functionally relevant evolutionary changes in bone proportions can be disentangled from evolutionary changes in body size (Pintore et al., 2024; Romano, 2017). This problem is compounded if the groups under consideration comprise samples of species occupying successively different ranges of body sizes, as occurred for a large part of synapsid history (Hellert et al., 2023; Kemp, 1982).

To address the aforementioned limitations, this study proposes a novel approach for calculating a size-independent measure of bone proportions (herein collectively referred to as "robusticity") for each taxon. This offers a means of quantifying the relationship between a trait and size on a per-species basis, facilitating assessment of evolutionary changes at every node in a phylogeny. Consider the bones of two different species i and j, with different absolute and relative dimensions, where size is measured by length l and a second dimension of interest is measured by d (Figure 3a). Together these two bones satisfy the common allometric scaling relationship of

$$d = kl^{\beta}, \tag{6}$$

where k is a constant of proportionality and β is the scaling exponent. The latter is uniquely defined by the dimensions of the two bones as

$$\beta = \frac{\log_{10}\left(\frac{d_i}{d_j}\right)}{\log_{10}\left(\frac{l_i}{l_j}\right)}, \tag{7}$$

or setting one of the species j as a point of reference ("ref"), the exponent for the other species i is

$$\beta_i = \frac{\log_{10}\left(\frac{d_i}{d_{\text{ref}}}\right)}{\log_{10}\left(\frac{l_i}{l_{\text{ref}}}\right)}. \tag{8}$$

Exponent β_i thus expresses the proportions for species i in relation to those of a reference; it is a geometric descriptor of the transformation required to go from one (reference) bone to another. This formulation has three important properties. Firstly, it does not carry any assumption or null hypothesis of how differently sized bones ought to scale with one another; departure from isometry is permissible as a pure consequence of changes in absolute size. In contrast, comparing absolute ratios implicitly forces the assumption of isometry on the dataset, wherein any departure from isometry must be interpreted as due to causes other than size. The second property is that the greater the value of β_i, the more robust bone i is, corrected for size in relation to the reference (Figure 3b). If $\beta_i > 1$, robusticity is greater than expected for the bone's length; if $\beta_i = 1$, robusticity is as expected for the bone's length (i.e., isometry); if $\beta_i < 1$, robusticity is less than expected for the bone's length; and if $\beta_i < 0$, the absolute dimension of d is less than that of the reference. There are also two trivial cases, namely

$$d_i = d_{\text{ref}} \longrightarrow \beta_i = 0, \tag{9a}$$

$$l_i = l_{\text{ref}} \longrightarrow \beta_i = \frac{d_i}{d_{\text{ref}}}. \tag{9b}$$

The third important property is that if two species i and j of differing absolute sizes ($l_i \neq l_j$) have equal exponents ($\beta_i = \beta_j$), they share the same allometric relationship with respect to the reference, and so are deemed equally robust for their size. Thus, in Figure 3b, the pair of species w and x fall on the same allometric curve and are equally robust, as are the pair of species y and z.

Calculation of β_i effectively permits the partitioning of a given bone's geometry into a size-related signal and a signal not related to size, such as functional, developmental, or phylogenetic effects. However, given that size may actually influence bone geometry at multiple levels of organization (e.g., changes in posture with increasing size; Biewener, 1989), this partitioning is most clearly made at the lowest level of organization, a "first order" assessment. By using an exponent-based measure of robusticity for each species, and evaluating how this changes from one species to the next, the evolution *of* allometry itself now comes under the spotlight of investigation. This is not to be confused with the study of "evolutionary allometry," which is simply interspecific scaling analyzed over evolutionary timescales.

In the present study, the reference used to compute β_i for each OTU was set with $l_{\text{ref}} = 1$ mm (i.e., all specimens have a greater length), and d_{ref} as the arithmetic mean of the ratio d_i/l_i across all OTUs. (Note that this does not take phylogenetic relatedness of the OTUs into account; it is simply a reference value used to compute a geometric transformation.) The value of β_i therefore still depends on the sample at hand, but unlike regression analyses, it is computed only with respect to the average proportions of the sample. Hence, in contrast to deriving species residuals from a sample-wide regression (Labonte et al., 2016; Romano, 2017), it is not influenced by trends within the dataset itself or how such trends may vary with size (i.e., differential scaling). As logarithms are involved in calculating β_i, in the subsequent analysis steps, any measurement recorded as zero (or negative, in rare cases where the greater trochanter projected

proximal to the femoral head) was arbitrarily set to 0.1% of l_i before proceeding. Size-corrected values for each raw trait H2a–H6b and F2a–F5b are reported for each OTU (where measurable) in Supporting Information S4.

2.5 | Analysis of stylopodial evolution

All calculations and analyses were undertaken using the "ape" (v5.7-1; Paradis & Schliep, 2019), "phytools" (v2.1-1; Revell, 2024), "caper" (v1.0.3; Orme et al., 2018) and "paleotree" (v3.4.5; Bapst, 2012) packages in the R statistical programming environment (R Core Team, 2021; see code in Appendix S1, Supporting Information). To examine the pattern of stylopod and body size evolution throughout synapsid history, ancestral state reconstruction (ASR) of the above raw and derived metrics was performed, using a residual maximum likelihood (REML) estimation procedure. To avoid basing inferences on a priori assumptions of structural or mechanical "optima," and in the absence of evidence to the contrary, a Brownian motion model of trait evolution was assumed. For body size, it should be noted that ASR of logarithmically transformed tip values may systematically underestimate the values at internal nodes (in the original, untransformed dimensions), although this concern is negated in the present study by focusing on relative, rather than absolute, changes in body size between adjacent nodes.

Phylogenetic relationships among the OTUs considered here were primarily represented by a single, fully resolved, time calibrated tree (Figure 1; see also Figures S1–S3). Its topology was based principally on the metatree of Hellert et al. (2023), supplemented with the results of Simões et al. (2022) and Berman (2013) for stem amniotes, Didier and Laurin (2021) for Ophiacodontidae and Sphenacodontidae, Kammerer and Ordoñez (2021) for Kannemeyeriformes, Sigogneau (1970), Kammerer (2016), and Bendel et al. (2018) for Gorgonopsia, Huttenlocker and Smith (2017), Huttenlocker and Sidor (2020), Sidor et al. (2021), and Kammerer (2023) for Therocephalia, and Kerber et al. (2022) for non-mammalian Prozostrodontia. The relationships and divergence times of extant mammals were generated using the TimeTree database (Hedges et al., 2006; data extracted on 1 February 2024). To facilitate this, seven extant taxa in the dataset were replaced by cogeneric species in the TimeTree database, which has no effect on the resulting phylogeny or divergence times generated: *Antechinus subtropicus* was replaced with *Antechinus stuartii*, *Canis lycaon* was replaced with *Canis lupus*, *Eulemur fulvus* was replaced with *Eulemur coronatus*, *Giraffa camelopardalis* was replaced with *Giraffa reticulata*, *Hapalemur griseus* was replaced with *Hapalemur aureus*, *Loris tardigradus* was replaced with *Loris lydekkerianus*, and *Smutsia temminckii* was replaced with *Smutsia gigantea*. The part of the phylogeny pertaining to extinct OTUs was temporally calibrated using first and last occurrence dates at the level of chronostratigraphic stage, derived from the Paleobiology Database (Alroy et al., 2012; data extracted on 30 January 2024, see Supporting Information S5). First and last appearance data were then used to estimate internal node ages using the timePaleoPhy function of the "paleotree" package (Bapst, 2012). To explore the effect of assumed branch lengths on the results of ASR, two different methods of temporal calibration were employed. The first used a minimum branch length approach, where all branches were forced to have a length of at least 1.0 Ma. The second used an equal partitioning algorithm (see also Brusatte et al., 2008), with the added constraint that the root of the tree had the same age as that in the minimum branch length tree, 322.6 Ma. Recently, new observations of the postcranium (Bishop & Pierce, 2024a) and neurocranium (Pusch et al., 2024) have lent further support to the possibility that Therocephalia is paraphyletic with respect to Cynodontia (see also Abdala, 2007; Abdala et al., 2019; Botha et al., 2007). Thus, a third phylogenetic tree was used in the present study, derived from the original equal algorithm calibrated tree, but with eutherocephalians set as more closely related to Cynodontia than lychosuchids or scylacosaurids (Figure S3).

For all three trees, ASRs of internal nodes were extracted for the stem lineage leading to Theria. In addition, reconstructions were extracted for the anomodont lineage (leading up to Stahleckeriidae); this represents the most speciose radiation of non-mammalian synapsids and encompasses a very wide range of body sizes (Angielczyk & Kammerer, 2018; Griffin & Angielczyk, 2019), which may have had important bearing on limb bone functional evolution.

The raw data underpinning this study almost entirely comprise manual measurements of physical specimens, mostly fossil material. Consequently, it is likely associated with an attendant level of measurement error, in addition to uncontrolled variation due to taphonomic deformation (although this was avoided wherever clearly apparent), intraspecific variation, and interspecific variability in ontogenetic stage or degree of ossification, among other factors. To explore the effect that error in the original dataset may have for downstream interpretations, ASR was performed in a Monte Carlo simulation framework. In each simulation, the underlying raw measurements in each taxon were perturbed by up to ±10% (multiplicative error), except for measurement F6, which was perturbed by up to ±5° (additive error) instead. Error was randomly drawn from a uniform distribution, and ASR was repeated for a total of 1000 simulation

replicates. Given the active attempt at selecting large, well-preserved specimens, the amount of potential error ascribed here is considered to be generous, and hence the ASR results recovered may be viewed as a conservative assessment of the "true" evolutionary patterns.

3 | RESULTS

Taxon-specific, size-corrected measurements for a representative selection of the metrics investigated are reported in Figure 4, to illustrate the spread of values obtained across time and various synapsid grades. ASRs using the equal-algorithm time-calibrated tree are reported in Figures 5–9. Results obtained using the other two phylogenies are reported in Figures S5–S14. Compared to the equal-algorithm tree, reconstructions using the minimum branch length tree differed mostly around advanced probainognathian cynodonts and basal mammals, but these differences were relatively minor and do not affect the broad-scale patterns described herein. Assuming a paraphyletic Therocephalia only influenced reconstructions in the immediate vicinity of the node Eutheriodontia, as might be expected.

3.1 | Diaphyseal dimensions

In both the humerus and femur, there is an overall trend of decreasing bone robusticity (when size corrected) from basal synapsids toward crown Theria (Figure 5). However, this trend is by no means monotonic or even in the rate of change (i.e., slopes of nodal values with respect to time) along the therian stem lineage, being

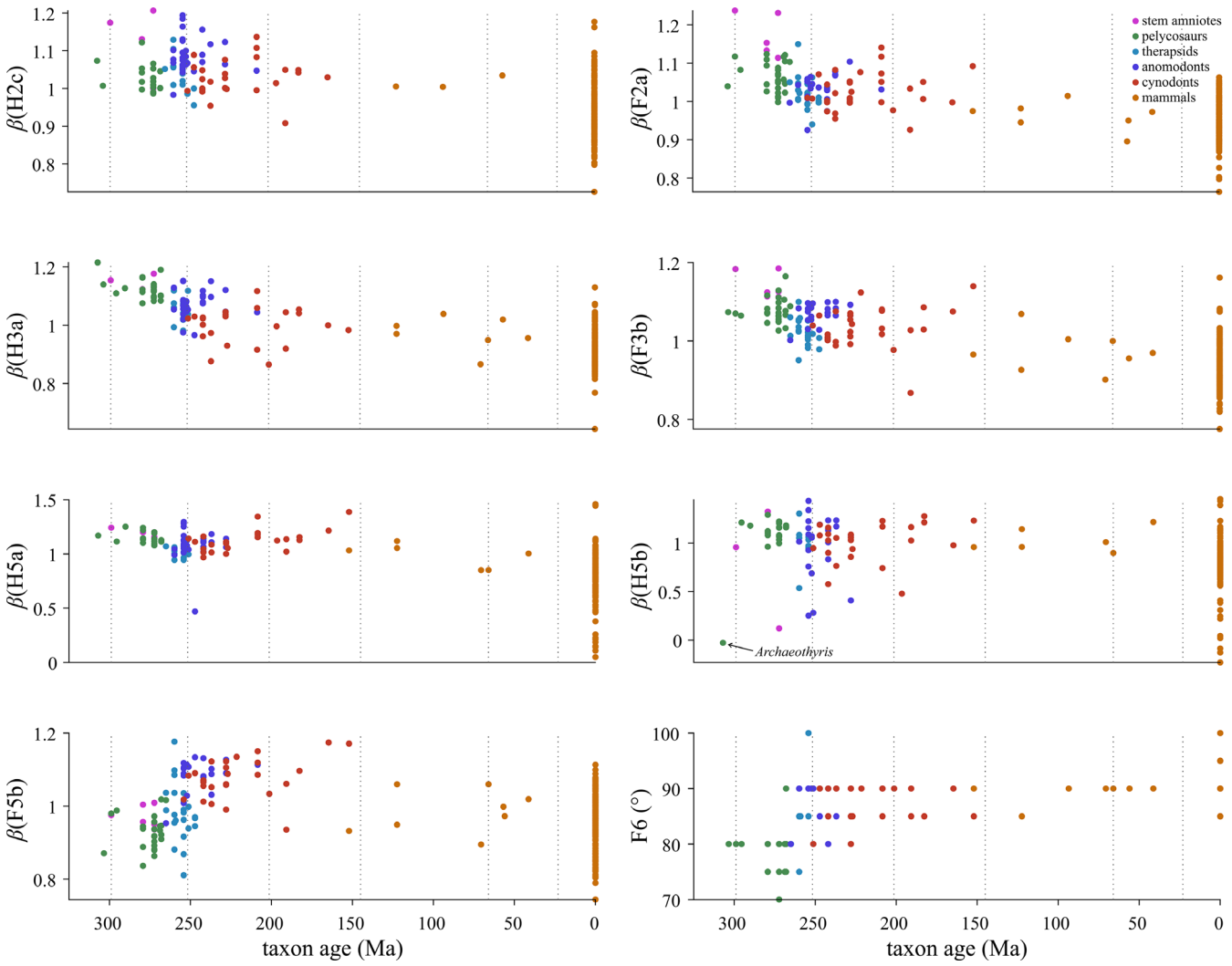

FIGURE 4 Raw taxon-specific measurements of a representative subset of metrics examined, illustrating the spread of data obtained across time and various synapsid grades. All data are reported as size-corrected β values, with the exception of F6, which is reported in its original measurement unit of degrees.

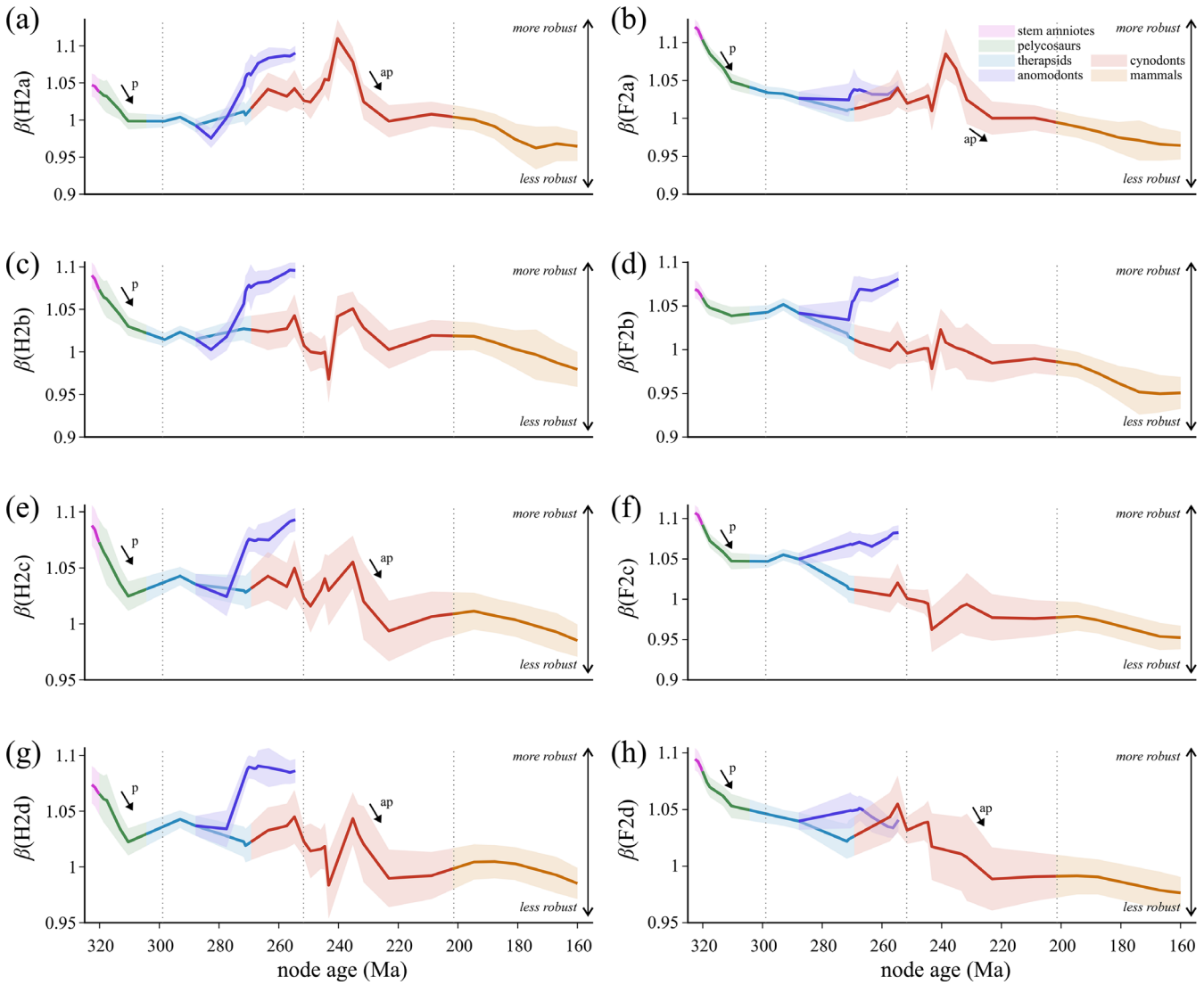

FIGURE 5 Nodal ancestral states reconstructed for size-corrected diaphyseal dimensions of the humerus (a, c, e, g) and femur (b, d, f, h) from stem amniotes to crown therians, using the equal-algorithm time-calibrated tree. Reported as the mean ± 2 standard deviation for each node across Monte Carlo simulations. Dotted lines denote the boundaries between geological periods (cf. Figure 1). See Figure 2 for descriptions of each measurement. Arrows indicate instances of particularly rapid decreases in robustness within "pelycosaurs" ("p") and advanced probainognathian cynodonts ("ap").

punctuated by several phases of increased robustness, particularly throughout much of non-mammalian Cynodontia. The most rapid decreases in robusticity appear to occur within "pelycosaurs" and advanced probainognathian cynodonts (Figure 5, arrows). In some metrics, basal therapsids are reconstructed as more robust than advanced "pelycosaurs" (Figure 5d,e,g), and basal mammals are reconstructed as more robust than advanced non-mammalian cynodonts (Figure 5a,c–e,g). In contrast to reconstructions for the therian stem lineage, the anomodont lineage exhibits an overall trend of increased diaphyseal robusticity on the line to Stahleckeriidae, especially in the humerus (Figure 5a,c,e,g).

3.2 | Epiphyseal dimensions

Paralleling the diaphysis, the epiphyses of both the humerus and femur exhibit an overall trend of decreasing linear dimensions from basal synapsids toward crown Theria (Figure 6). As with diaphyseal dimensions, the pattern of change here is generally not monotonic. Further, anomodonts again illustrate the opposite pattern, with a trend toward increased epiphyseal robusticity in the humerus and (distal) femur. In the proximal humerus, both the articular surface (Figure 6a) and overall epiphysis (Figure 6c) start becoming narrower within "pelycosaurs" and approaches therian-like values (i.e., the reconstructed state at the crown Theria node)

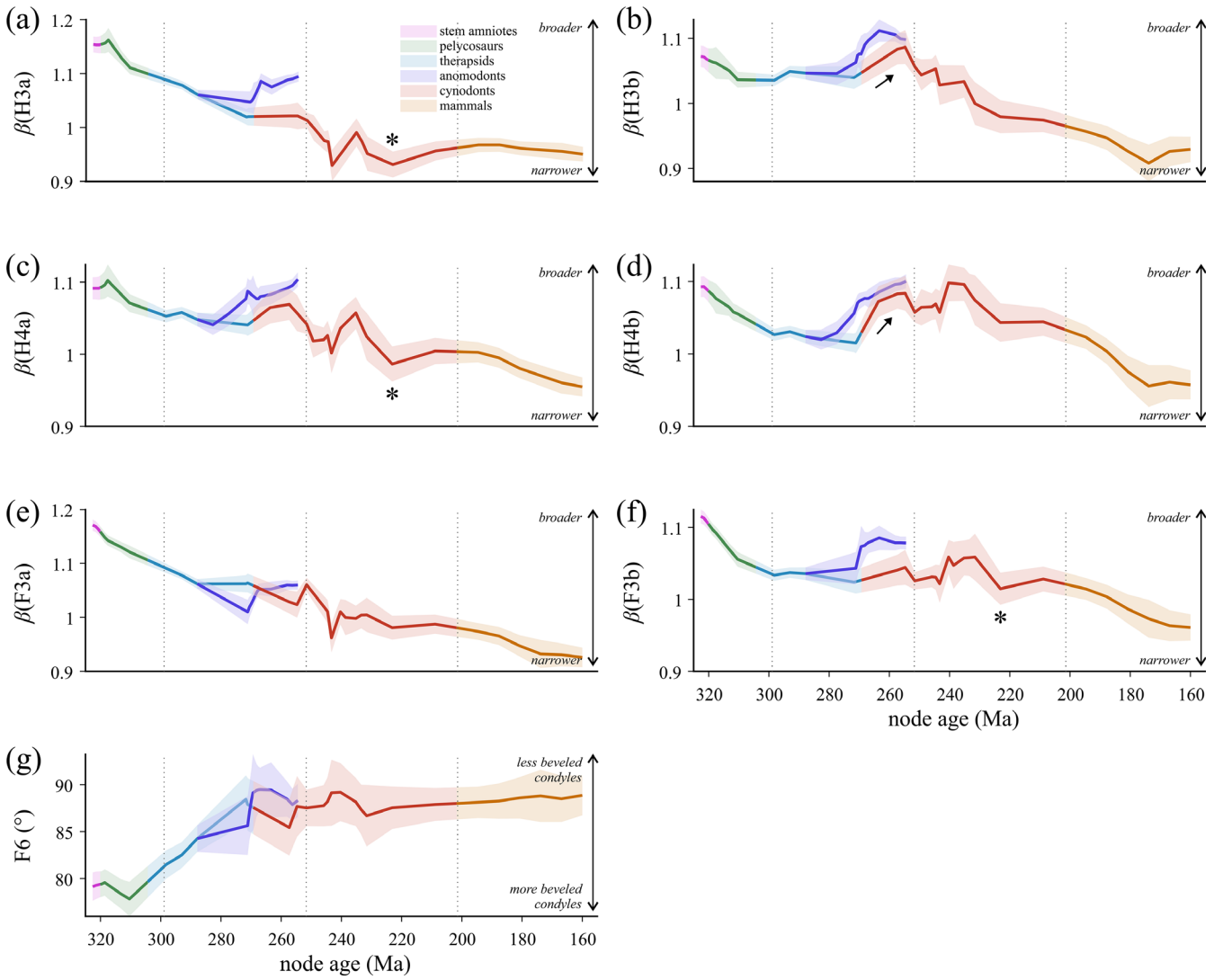

FIGURE 6 Nodal ancestral states reconstructed for size-corrected epiphyseal dimensions of the humerus (a–d) and femur (e–g) from stem amniotes to crown therians. Conventions as in Figure 5. See Figure 2 for descriptions of each measurement. Arrows in (b) and (d) indicate a transient reversal to more robust dimensions in basal cynodonts; asterisk denotes the Mammaliaformes node.

around Mammaliaformes. Notably, some humeral dimensions at Mammaliaformes are reconstructed as less robust compared to preceding or succeeding nodes (Figure 6, asterisks). In the distal humerus, the overall trend of phyletic decrease in dimensions is interrupted by a prominent reversal toward broader dimensions in basal cynodonts (Figure 6b,d, arrow). Whereas the distal condyles progressively decrease in breadth from Eucynodontia onward (Figure 6b), total epiphyseal width remains relatively high until the origin of Mammalia (Figure 6d), indicating increased relative development of the epicondyles (see also below).

In the femur, femoral head width exhibits a nearly monotonic decrease through time (Figure 6e). In contrast to most other dimensions, the width of the femoral head in anomodonts does not undergo a net increase over time. Femoral condyle width (Figure 6f) exhibits a sustained decrease from stem amniotes through to basal therapsids, but thereafter it remains largely static along the stem lineage until the appearance of crown mammals, upon which it again decreases on the line to Theria. Starting from a strongly angled disposition in stem amniotes and "pelycosaurs," beveling of the femoral condyles reduces in early therapsids to reach therian levels in theriodonts and, independently, dicynodont anomodonts (Figure 6g).

3.3 | Humeral muscle attachments

Starting out as a very well-developed structure in stem amniotes and basal "pelycosaurs," the entepicondyle

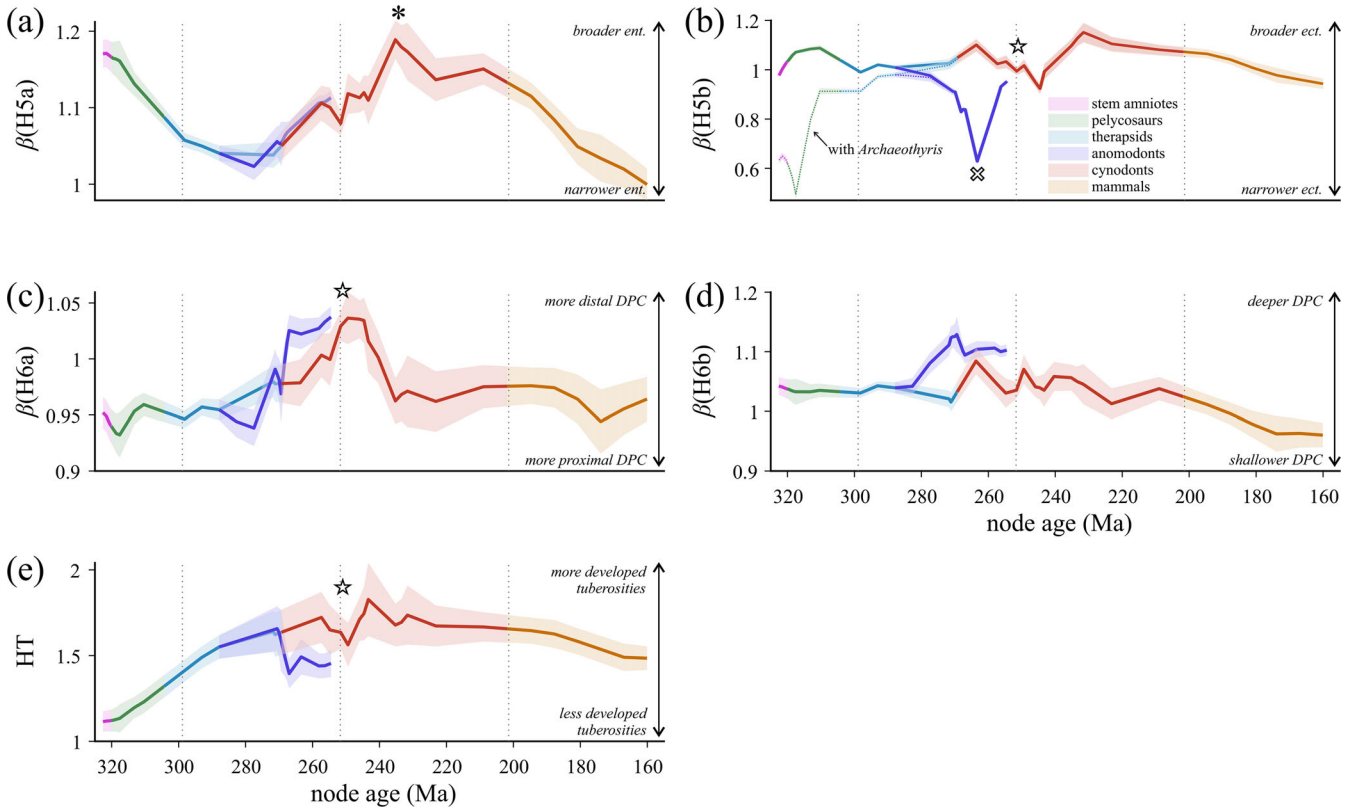

FIGURE 7 Nodal ancestral states reconstructed for size-corrected dimensions of the humerus related to muscle attachment, from stem amniotes to crown therians. Conventions as in Figure 5. See Figure 2 for descriptions of each measurement. In (b), the results are plotted for reconstructions both including and excluding the ophiacodontid *Archaeothyris*, which is apomorphic in regard to the ectepicondyle (Reisz, 1972). DPC, deltopectoral crest; ect., ectepicondyle; ent., entepicondyle. Symbols denote the following nodes: cross, Dicynodontoidea; star, Eucynodontia; asterisk, advanced Probainognathia.

progressively reduces in advanced "pelycosaurs" and therapsids, reaching minimal development in Eutheriodontia (Figure 7a). Remarkably, this trend is reversed and entepicondylar breadth progressively increases within cynodonts, with advanced probainognathians exhibiting a comparable degree of development to that of stem amniotes (Figure 7a, asterisk); it only reduces to its modest size in therians within crown mammals. A similar reversal toward progressively greater entepicondylar development appears in parallel within dicynodont anomodonts. In contrast to the entepicondyle, the ectepicondyle exhibits a less drastic history of transformation, with a slight increase from basal therapsids to advanced cynodonts interrupted by a transient phase of decreased development within early eucynodonts (Figure 7b, star), prior to a gradual decrease on the line to Theria. The ectepicondyle of anomodonts gradually reduces in development, reaching a minimum around Dicynodontoidea (Figure 7b, cross), before increasing in size again on the line to Stahleckeriidae. Of note, the pattern reconstructed for stem amniotes, "pelycosaurs" and even basal therapsids is strongly influenced by the condition in the ophiacodontid *Archaeothyris* (Figure 7b), which although not the basalmost member of the family is by far the oldest taxon in the dataset (Figure S1). The ectepicondyle of *Archaeothyris* is vertically (dorsally) situated above the radial capitellum, rather than anterior to it (see Reisz, 1972, figure 9), which is apomorphic (measure H5b is zero in this taxon). By contrast, the more basal ophiacodontid *Clepsydrops* exhibits the typical anterior disposition of the ectepicondyle (Romer & Price, 1940), but appropriate specimens were unable to be measured for this study. Excluding *Archaeothyris* results in a less pronounced pattern of change reconstructed for the early part of synapsid history (Figure 7b).

In the proximal humerus, the apex of the deltopectoral crest progressively shifts more distally from basal synapsids to eucynodonts (Figure 7c, star), after which it becomes more proximally situated in more advanced cynodonts, thereafter remaining at a similar position on the line to Theria. The shift toward a progressively more distal position is also observed in the anomodont lineage. The height of the deltopectoral crest remains fairly constant in development from stem amniotes through to

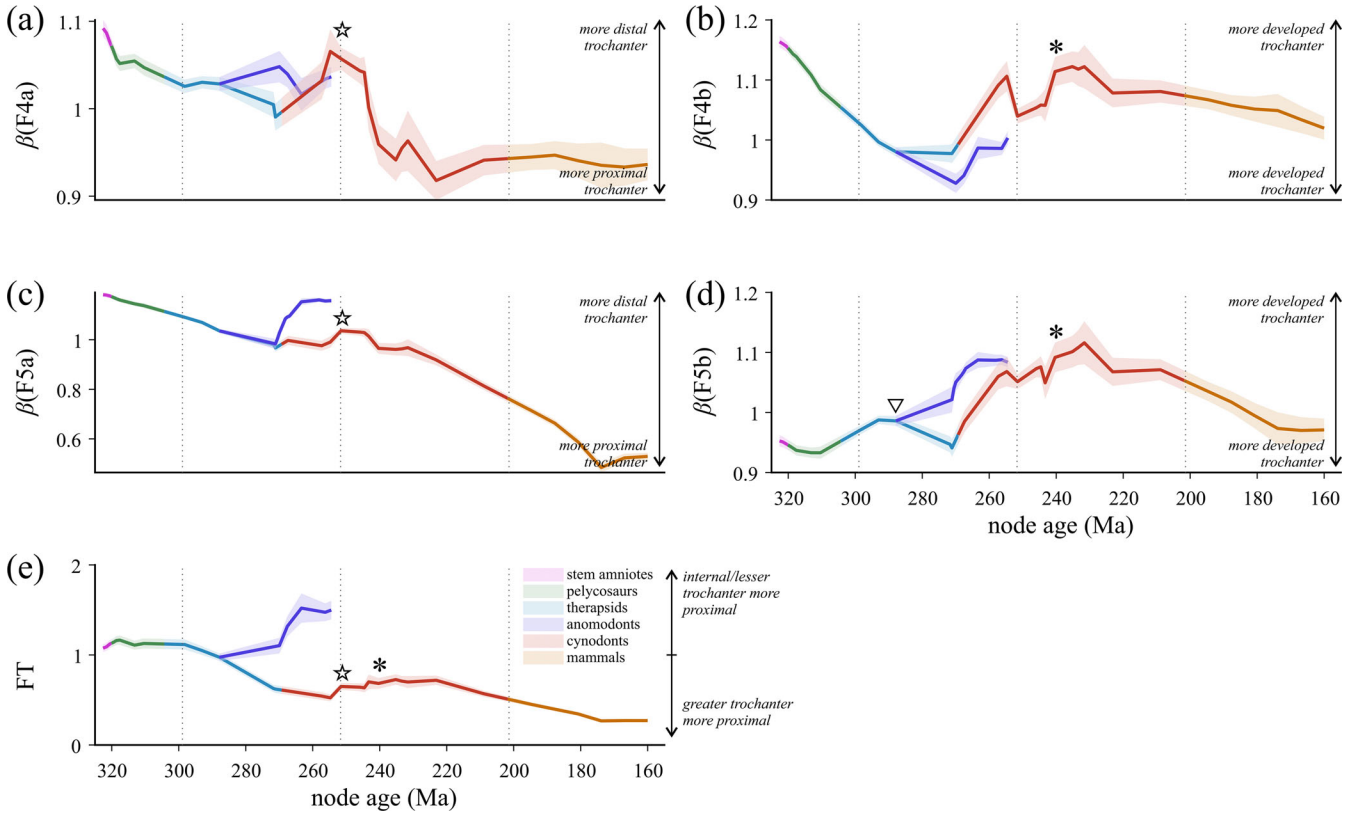

FIGURE 8 Nodal ancestral states reconstructed for size-corrected dimensions of the femur related to muscle attachment, from stem amniotes to crown therians. Conventions as in Figure 5. See Figure 2 for descriptions of each measurement. Symbols denote the following nodes: triangle, Neotherapsida; star, Eucynodontia; asterisk, Prozostrodontia.

crown mammals, notwithstanding minor transient fluctuations (Figure 7d). It progressively expands in dicynodont anomodonts, but diminishes within mammals on the line to Theria, where its morphology is more aptly described as a "crest" than a "blade." The development of attachments for the supracoracoideus (or homologs) and subscapularis muscles progressively increases from stem amniotes to eucynodonts (Figure 7e, star), even before the appearance of a distinct greater tuberosity in basal cynodonts (Bishop & Pierce, 2024a). The development of these attachments relative to the humeral head then progressively decreases within crown mammals, and, independently, in dicynodont anomodonts.

3.4 | Femoral muscle attachments

From basal synapsids toward crown Theria, the anteroventral trochanter exhibits an overall trend of becoming more proximally sited (Figure 8a). Superimposed upon this is a transient shift to a more distal location at the origin of cynodonts, which reaches an acme around Eucynodontia (Figure 8a, star) prior to a proximal shift toward a therian-like position in advanced probainognathians. Paralleling changes in proximodistal position, the development (height) of the trochanter progressively decreases from stem amniotes onward, but re-expands in early cynodonts (Figure 8b), coinciding with the reconfiguration of hip muscle insertions and the internal trochanter "becoming" the lesser trochanter (Bishop & Pierce, 2024b). The trochanter is most strongly developed in prozostrodontian cynodonts (Figure 8b, asterisk), but thereafter gradually decreases on the line to therians.

The insertion of the IF exhibits a nearly monotonic trend of becoming more proximally sited on the line to therians, save for a small transient distal shift around Eucynodontia (Figure 8c, star); the insertion also shifts distally in dicynodont anomodonts. The lateral "height" of the insertion increases from "pelycosaurs" to neotherapsids (Figure 8d, triangle) as a distinct greater trochanter evolves, a trend continued within anomodonts. In contrast, the greater trochanter reduces in development in theriodonts, but expands in early cynodonts, reaching maximal development in prozostrodontians (Figure 8d, asterisk) prior to a gradual reduction on the line to Theria.

In terms of the relative proximodistal positioning of muscle insertions (Figure 8e), there is an overall phyletic

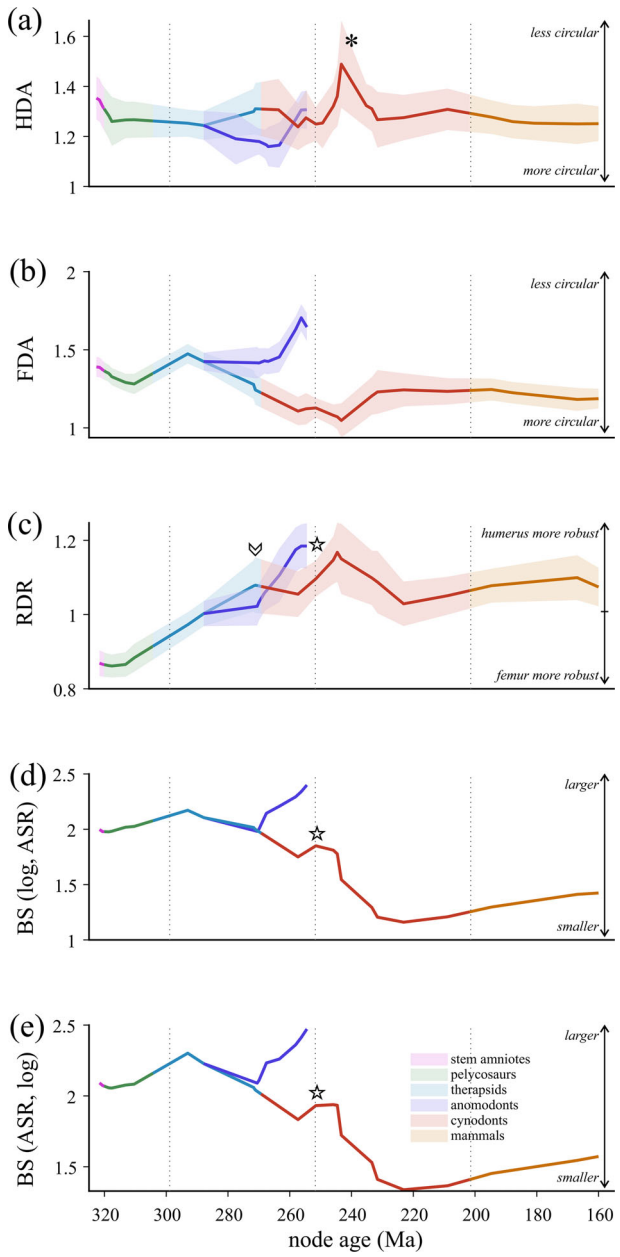

FIGURE 9 Nodal ancestral states reconstructed for derived metrics from stem amniotes to crown therians. (a) Humeral diaphyseal asymmetry. (b) Femoral diaphyseal asymmetry. (c) Relative diaphyseal robusticity. (d) Body size, wherein data was logarithmically transformed prior to ancestral state reconstruction. (e) Body size, wherein untransformed data was used for ancestral state reconstruction, and the resulting mean and standard deviation for each node then logarithmically transformed. In (d) and (e), note the transient increase in body size around Eucynodontia, superimposed on an otherwise sustained trend of miniaturization from early therapsids to advanced probainognathian cynodonts. Conventions as in Figure 5. Symbols denote the following nodes: chevron, Eutheriodontia; star, Eucynodontia; asterisk, Prozostrodontia.

trend of the greater trochanter (or its precursor attachment area) becoming more proximally positioned compared to the anteroventral trochanter in later diverging synapsids. This trend is punctuated by a period where the apices of the two trochanters are more closely level with one another, in eucynodonts and basal prozostrodontians (Figure 8e, star and asterisk). As both the lesser and greater trochanters of cynodonts progressively shift proximally over time (Figure 8a,c), the shift is more marked in the lesser trochanter (Figure 8a); the transient increase in the reconstructed value for FT likely reflects a stronger proximal shift of the lesser trochanter during this period. In contrast to the therian stem lineage, the apex of the internal trochanter becomes more proximally sited than that of the greater trochanter in the anomodont lineage.

3.5 | Other derived metrics

Diaphyseal asymmetry in the humerus (Figure 9a) and femur (Figure 9b) are largely consistent across time, with no clear trend from basal "pelycosaurs" to crown therians. Increases or decreases in asymmetry at one point in the stem lineage are reversed at subsequent stages. Humeral asymmetry is transiently high in basal prozostrodontians (Figure 9a, asterisk), but otherwise is quite consistent across Cynodontia. Whereas the humerus of advanced dicynodonts is marginally more asymmetric compared to the ancestral condition for Anomodontia as a whole, femoral asymmetry exhibits a sustained increase throughout the anomodont lineage, producing some of the most asymmetric femoral diaphyses across the entire sample of taxa. Elsewhere within therapsids, femoral asymmetry is highest around Eutherapsida, decreasing nearly monotonically up to eucynodonts, which have nearly circular diaphyses.

Relative diaphyseal robusticity exhibits a clear trend throughout synapsid evolution (Figure 9c), with the humerus becoming progressively more robust than the femur on the line to therians and, convergently, on the line to advanced dicynodonts. Therian-like values of RDR are reached as early as eutheriodonts (Figure 9c, chevron), continuing into an acme in basal eucynodonts (Figure 9c, star). The semi-quantitative assessment of body size (or more precisely, logarithmically transformed body size) on the therian stem lineage identifies a peak in early therapsids that subsequently decreases toward advanced probainognathian cynodonts, with a gradual increase thereafter on the line to Theria (Figure 9d). Anomodontia exhibits a monotonic increase in body size following the appearance of dicynodonts. Notably, the decrease in body size from early therapsids to advanced cynodonts is punctuated by a transient increase in size around Eucynodontia (Figure 9d, star). Re-running ASR using the original (un-transformed) values of body size and then logarithmically transforming the reconstructed nodal values afterwards did not substantially alter the qualitative pattern recovered (Figure 9e).

4 | DISCUSSION

The transition from sprawled to erect limb postures in synapsids entailed important shifts in numerous aspects of locomotor biomechanics, including musculoskeletal anatomy, joint mobility, muscle control strategies, bone loading regimes, and the relative functions of the fore- and hindlimbs. These might be expected to have left a signature on skeletal structure and its evolution through time. Drawing upon a large dataset of humeri and femora spanning the entirety of synapsid evolution, the present study sought to evaluate the extent to which evolutionary transformation in biomechanically relevant measures of bone proportions (once corrected for size) is consistent with presumed functional shifts. Four such shifts were examined: (1) a change in bone loading regime, from torsion- to bending-dominant; (2) a realignment of the bones, and joint and muscle forces, closer to the sagittal plane; (3) changes in the efficacy of major shoulder and hip muscles; and (4) the forelimb acquiring a greater role in body weight support. Observed evolutionary patterns in bone geometry can provide a lens to examine how these shifts occurred.

4.1 | Overarching patterns of structural evolution

Although this study focuses on shifts in locomotor biomechanics as interpreted from bony structure, it is important to also consider the patterns of evolutionary change evidenced by the data, for both individual metrics and as a collective whole. Appreciating the broader evolutionary context can provide a more nuanced backdrop for evaluating the functional implications of changes in stylopod structure, as explored in the succeeding sections. ASRs reveal a complex pattern of structural transformation along the stem lineage leading to therian mammals. While the changes that took place between basal synapsids and crown therians are largely consistent with hypothesized shifts in mechanics between these two evolutionary endpoints (see below), these changes were rarely straightforward. Across individual anatomical traits, there is considerable diversity in the inferred patterns of change, which are frequently nonlinear and temporally asynchronous with one another. Thus, whereas some aspects of (size-corrected) bony geometry exhibit a nearly monotonic trend on the line to Theria (e.g., humeral and femoral head widths, IF insertion on the femur; Figures 6a,e and 8c), many others exhibit reversals at some point along the stem lineage, even if only transient (e.g., diaphyseal robustness and asymmetry, entepicondyle breadth, deltopectoral crest extent and depth, puboischiofemorales insertion on the femur; Figures 5, 7a,c,d and 8a,b). In addition to the asynchronous timing of anatomical shifts, few of the metrics examined here appear to reach (size-corrected) therian-like proportions prior to the origin of Theria itself. In some instances, therian-like levels are reached as early as Theriodontia (e.g., femoral condyle beveling, ectepicondylar width; Figures 6g and 7b), whereas in others, they are not reached until the appearance of Theria (e.g., epiphyseal widths, deltopectoral crest depth; Figures 6b–d and 7d). As evidenced by the humerus and femur, assembly of the collective suite of traits ancestral for crown Theria was apparently piecemeal, protracted, and relatively late in its completion (see also Bishop & Pierce, 2024c; Brocklehurst et al., 2025; Jones et al., 2024).

Taken at face value, these patterns imply functional mosaicism, wherein various synapsid lineages explored subtly different "styles" of locomotor mechanics on the line to Theria. Such diversity in locomotor evolution is particularly well illustrated by Anomodontia, which exhibited a combination of trends that both paralleled (e.g., femoral condyle beveling, deltopectoral crest extent; Figures 6g and 7c) and strongly departed from (e.g., humeral diaphyseal robusticity, femoral diaphyseal asymmetry; Figures 5a,c,e,g and 9b) those reconstructed for the therian stem lineage. As a long-lived, highly diverse clade of non-mammalian synapsids (Angielczyk & Kammerer, 2018; King, 1988, 1990), a relatively large sampling of anomodonts was possible in the present study, facilitating an assessment of how individual clades may follow their own evolutionary trajectory once splitting from the main stem lineage. Future investigation is warranted to determine how these divergent evolutionary trajectories correspond to differences in locomotor mechanics between anomodonts and other non-mammalian synapsid clades.

4.2 | Transformations related to bone loading regime

Humeral and femoral diaphyseal dimensions generally decrease from early synapsids to therians (Figure 5): later-diverging taxa tend to possess less robust bones. All else being equal, bones with more robust diaphyses have a greater resistance to applied bending and torsional moments (Biewener, 1992; Currey, 2002; Wainwright et al., 1976), although resistance to axial loads remains unaltered (assuming equal cross-sectional areas of cortical bone; see below). More robust bones are therefore better suited to postures, kinematics, and muscle control patterns that engender forces less aligned with the long-

axis of the bone, a scenario typifying sprawling locomotion among quadrupeds (Blob, 2000, 2001; Blob & Biewener, 2001; Butcher & Blob, 2008; Hutchinson & Gatesy, 2000; Sheffield et al., 2011; Sheffield & Blob, 2011). Although bending is experienced across a diverse array of extant taxa, marked torsional loading appears to primarily be a characteristic of sprawled locomotion (Blob et al., 2014; Blob & Biewener, 1999; Butcher et al., 2008; Sheffield et al., 2011; Sheffield & Blob, 2011; Young et al., 2017), and independently also in bipedal birds (Biewener et al., 1986; Carrano & Biewener, 1999; Main & Biewener, 2007). Torsion induces shear stress, the form of stress that bone tissue tends to be weakest in (Currey, 2002), and hence diaphyseal geometry may preferentially be optimized to resist torsional loading over bending or axial compression (Bishop et al., 2018b; Blob, 2000; Doube et al., 2012). Given these considerations, the evolutionary reduction of diaphyseal robusticity on the line to therians is consistent with a posture-mediated shift in bone loading mechanics within synapsids, from torsion- to bending- and compression-dominant.

In contrast to overall dimensions, observed diaphyseal asymmetry in the humerus (HDA) and femur (FDA) is not consistent with the expected shift from torsion- to bending-dominant loading (Figure 9a,b). If bending loads are more prevalent, basic beam theory would lead to the expectation that diaphyses should be more asymmetric (less circular) in cross-section, with the "major axis" of the section, corresponding to minimal second moment of area, aligned with the direction of bending (Beer et al., 2012; Wainwright et al., 1976). Yet, HDA does not appreciably change across the span from early synapsids to crown therians. Furthermore, FDA decreases from Eutherapsida to Eucynodontia (i.e., the femoral diaphysis becomes more circular), a result broadly mirroring the observations of Blob (2001; made on a smaller sample of specimens and taxa), and more broadly exhibits a small net decrease across the entire span from basal synapsids to crown therians. This parallels the observation noted in Section 1, that extant sprawling saurians and erect carnivorans show little difference in FDA (Bertram & Biewener, 1990; Blob, 2000). Moreover, experimental studies highlight that diaphyseal shape (asymmetry, in this case) may not always be a reliable indicator of the nature of in vivo bone loading or bending direction (Bertram & Biewener, 1988; Biewener & Taylor, 1986; Butcher et al., 2008; Demes et al., 1998, 2001; Lieberman et al., 2004; Main & Biewener, 2004; Pearson & Lieberman, 2004; Wallace et al., 2014). Interpretations of the significance of stylopod external diaphyseal shape in extinct synapsids, especially asymmetry and the axis of maximal bending strength, should therefore be made with great caution, or perhaps avoided altogether.

4.3 | Transformations related to alignment of joint and muscle forces

In a similar fashion to the diaphyses, humeral and femoral epiphyseal dimensions generally decrease from early synapsids through to therians (Figure 6a–f). The width of the ends of a bone, especially the articular surfaces, influences the capacity for joint moment control by active and passive forces, but can also influence the possible range of joint mobility (Currey, 2002). The observed trends toward more gracile stylopod epiphyses thus probably indicate progressively increased joint mobility at the expense of reduced efficacy of passive contributions (via ligaments or bony stops) to joint moment balance, especially in terms of long-axis rotation (see also Bishop et al., 2023 for a discussion of "hard" and "soft" mechanisms of joint control). This likely required compensation by a greater reliance on active forces from the musculature. The phyletic trend toward a lower efficacy of (and reduced reliance upon) passive joint control could also be facilitated by a reduced need for the control of off-axis moments in the first instance, whereby the external joint moments induced by gravity and limb motions are better aligned with the axes about which musculature is suited to functioning. The most straightforward way this could be achieved is by bringing limb bones, limb motions, and internal and external forces more into alignment with a single common plane, the parasagittal plane.

Such a scenario appears particularly relevant to the knee joint, where most muscles are suited principally to controlling flexion–extension moments. In addition to reducing epiphyseal breadth, the distal femoral condyles become less beveled (skewed) over time, with a therian-like level of minimal beveling attained as early as eutheriodonts (Figure 6f). Although skewed joint orientations are relevant to keeping the pes facing anteriorly during locomotion in sprawled poses (Rewcastle, 1980, 1983), they also partition external joint moments across multiple anatomical axes; or conversely, they enable muscular forces to contribute to moment control about multiple axes. Reduction of beveling of the distal femur, in tandem with a reduction in epiphyseal breadth, may therefore be interpreted as also being linked to a greater alignment of knee external joint moments with the direction of muscular forces, which are best suited to controlling flexion–extension moments. A similar argument can also be made for the elbow joint. Again, as external joint moments become more aligned with the flexion–extension plane, the need for generating stabilizing moments in abduction–adduction or long-axis rotation reduces, in turn reducing the need for bony geometry supporting those requirements, such as large ent- and ectepicondyles (Fujiwara & Hutchinson, 2012; Nakai &

Fujiwara, 2023). Nevertheless, within stem therians, the humero-ulnar joint developed a characteristic trochlear morphology, probably conferring a novel level of passive stability to the elbow against motions away from the flexion–extension plane (Jenkins Jr., 1973).

Despite these overarching trends from early synapsids to crown therians, the distal humerus experiences a notable increase in breadth throughout non-mammalian cynodonts (Figure 6d). Although articular surface breadth transiently increases in basal cynodonts (Figure 6b), the primary driver of this pattern appears to be sustained re-expansion of the entepicondyle, with advanced probainognathians possessing some of the broadest entepicondyles across the whole sample (Figure 7a, asterisk). As the entepicondyle broadens far more than the adjacent radio-ulnar articular surface, this suggests that the proximate driving factor was not simply related to passive maintenance of stability at the elbow joint. Instead, given that the entepicondyle serves as the origin for the forearm flexor muscles (Bishop & Pierce, 2024a), its expansion implicates enhanced muscular control of wrist flexion, and possibly also forearm pronation, either through larger muscle volumes (strength) or moment arms (leverage). One plausible reason for such enhanced muscular control is increased use of the forelimbs in digging or other forceful behavior. Greatly expanded entepicondyles frequently typify the humerus of extant fossorial mammals (e.g., Edwards, 1937; Gambaryan et al., 2015; Warburton, 2006), as well as those of some dicynodonts widely regarded as fossorial (Cluver, 1978; Cox, 1972). Indeed, some cynodonts are presumed to have used, if not directly dug, burrows in the Triassic (Damiani et al., 2003; Fernandez et al., 2013; Groenewald et al., 2001). Accordingly, fossorial habits appear to have left a significant overprint on the trend of humeral evolution along the therian stem.

4.4 | Transformations related to shoulder and hip musculature

The reorganization of fore- and hindlimb musculature in synapsids on the line to mammals has a long history of investigation (see Bishop & Pierce, 2024a, 2024b and references cited therein), as does the potential functional consequences of evolutionary shifts in muscular anatomy (e.g., Bishop & Pierce, 2024c; Boonstra, 1967; Colbert, 1948; Gregory, 1926; Guignard et al., 2019; Jenkins Jr., 1971b; Kemp, 1978, 1982; King, 1981; Ray, 2006; Sullivan et al., 2013). Yet, the direct connection between changes in muscle function and modifications of humeral or femoral structure itself has been little addressed (e.g., Brocklehurst et al., 2025; Guignard et al., 2019; Jenkins Jr., 1971b; Kemp, 1982; Sullivan et al., 2013). Without additional information on habitual limb postures, transformation in the function of specific muscles on the line to mammals cannot be discerned from the results of the present study alone. Nevertheless, important insights can be gained into the efficacy of key hip and shoulder muscles in performing their functions, whatever those may be. A temporary increase in the distal extent of the deltopectoral crest of the humerus in advanced therapsids and non-prozostrodontian cynodonts, and independently in dicynodont anomodonts (Figure 7c), indicates increased mechanical advantage for the pectoralis, the primary depressor of the shoulder. This would tend to produce more forceful, but slower, movements, and is consilient with the inferred increased use of the forelimbs in digging or related behaviors in cynodonts (see above). A long-term trend of decreasing height of the deltopectoral crest along the stem lineage (Figure 7d) indicates that the pectoralis had reduced capacity for effecting long-axis rotation of the humerus, irrespective of how it contributed to controlling forelimb elevation–depression (Brocklehurst et al., 2022). As noted above, attachments for the supracoracoideus and subscapularis muscle masses progressively expand along the stem lineage (Figure 7e), prior to the first osteological indicators of supracoracoideus reorganization around Cynodontia (Bishop and Pierce, 2024a). This discord may indicate subtle changes in supracoracoideus arrangement or function in advanced "pelycosaurs" and non-cynodont therapsids (e.g., increased size and importance), prior to a more pronounced transformation within cynodonts, but such interpretation must await quantitative testing via mechanistic, musculoskeletal modeling approaches (Bishop et al., 2021; Bishop & Pierce, 2024c; Brocklehurst et al., 2022).

In the hindlimb, the apices of the anteroventral and greater trochanters (or their homologous areas of muscle attachment) show a common long-term trend, becoming progressively more proximally positioned on the femur on the line to Theria (Figure 8a,c). This does not clarify shifts in differential muscle control strategies, but does indicate a collective trend toward the execution of faster, but less forceful, movements in stance and swing phase, particularly in the dorsoventral and anteroposterior directions. Changes in the height of the anteroventral trochanter can be reconciled with reconfiguration of the hip musculature in cynodonts (Figure 8b; Bishop & Pierce, 2024b). In the anomodont lineage, recovered trends for the anteroventral trochanter ("internal trochanter") should be viewed with some caution, as the trochanter is typically poorly expressed, if at all, in most dicynodonts (Bishop & Pierce, 2024b). Changes in the height of the greater trochanter (Figure 8d) are difficult to interpret in isolation, since this may affect the efficacy

of the IF mass in generating movement about multiple axes, including long-axis rotation. Again, a quantitative assessment via musculoskeletal modeling can clarify the situation. Lastly, it is worth noting that an additional femoral trochanter evolved within Mammaliaformes, the third trochanter, which persists in many extant mammal groups (Bishop & Pierce, 2024b). The third trochanter was not measured in the present study, but in many extant placentals (e.g., rodents, lagomorphs, tupaiids, and perissodactyls), it is more laterally positioned with respect to the femoral head compared to the greater trochanter. This may mean that in these taxa the attaching muscle (gluteus maximus) plays a greater role in effecting hip abduction (elevation) or long-axis rotation in relation to those muscles inserting on the greater trochanter (gluteus medius and minimum, and potentially others).

4.5 | Transformations related to body mass and its distribution

While only semi-quantitative, the reconstructed pattern of (logarithmically transformed) body size along the therian stem lineage obtained here is in general agreement with prior assessments (Brocklehurst & Brink, 2017; Hellert et al., 2023; Kaiuca et al., 2024), illustrating a long-term decrease from a peak around early therapsids toward crown Theria. Perhaps the most noteworthy aspect is a small, transient increase around Eucynodontia (Figure 9d,e, star), interrupting an otherwise sustained trend of miniaturization from Neotherapsida to Mammaliamorpha, a pattern that was also recovered by Kaiuca et al. (2024) in an assessment of cranial, mandibular, and postcranial dimensions across cynodonts. This transient increase reflects the fact that many basal eucynodonts (including *Cynognathus*, *Diademodon*, *Trucidocynodon*, *Aleodon*, and *Chiniquodon*) are among the largest known of all non-mammalian cynodonts (Kaiuca et al., 2024). On current evidence, the origin of Eucynodontia is inferred to approximately coincide with the Permian–Triassic mass extinction (Figures S1–S3), which saw a temporary reduction in eutheriodont body sizes via selective extinction of medium- and large-bodied carnivorous taxa (Huttenlocker, 2014). This invites speculation as to whether the associated ecological upheaval temporarily paused, or even reversed, selection pressures acting on the stem lineage, leading to a minor radiation of larger-bodied taxa. Additional fossil material of basal eucynodonts, especially from the earliest Triassic, would prove highly useful in testing this scenario. Just as importantly, increased efforts to derive reliable estimations of absolute body mass in non-mammalian synapsids, which work well across a diversity of body forms, will increase the quantitative rigor of such analyses (Wright et al., 2024).

The overall trend reconstructed for RDR (Figure 9c) is consistent with an inferred anterior shift in the whole-body center of mass on the line to therians: the humerus becomes more robust as it supports a progressively greater portion of body weight. Therian-like values of RDR appear as early as theriodonts, consistent with the strongly reduced tails and very large heads of many of these animals (Broili & Schröder, 1935; Colbert, 1948; Fourie & Rubidge, 2007, 2009; Kemp, 1986; Pravoslavev, 1927; Tatarinov, 2004; von Huene, 1950; Watson, 1931). While the present results suggest that RDR is a faithful proxy of body mass distribution, its accuracy or precision as a predictor remains to be demonstrated. Such an exercise would first require the creation of volumetric models for quantitative estimation of whole-body center of mass position in a diverse array of taxa (Bishop et al., 2020; Morato et al., 2008; Romano & Manucci, 2021; Romano & Rubidge, 2021; Wright et al., 2024). Until such a demonstration is made, minor phyletic increases or decreases in RDR, such as those occurring in non-mammalian cynodonts (Figure 9c), should be interpreted tentatively. Small node-to-node differences may indicate subtle shifts in whole-body center of mass location or alternatively indicate variable locomotor behavior or diverse, ecologically relevant functions of the limbs (e.g., digging; see above).

4.6 | Caveats

Two important sets of limitations should be borne in mind when considering the results of the present study.

4.6.1 | Measurements

The primary data underpinning this study are measurements of external bone dimensions. In less well ossified specimens, the measurements made may be significant underestimates of the true dimensions of the bone. For example, humeral tuberosities or ent- or ectepicondyles may be furnished with fibrocartilage, and proximodistal bone length (used here to normalize the majority of measurements) will be greater in vivo due to extensions of hyaline cartilage (Holliday et al., 2010; Molnar, 2021; Tsai & Holliday, 2015). Systematic errors may thus exist in comparisons involving taxa of markedly varying levels of ossification (consider dicynodonts v. sphenacodontids). Although Monte Carlo simulations suggest that the broad phyletic trends identified here would be robust to such error, interpreting finer-scale changes may be more subject to uncertainty.

Irrespective of ossification status, the measurements of bone geometry examined here only concern the

external dimensions of the humerus and femur. Although these can provide insight on various biomechanically relevant aspects of locomotor behavior, internal geometry will also contain functionally relevant information. For instance, the amount and distribution of cortical bone in the diaphyses is intimately related to a bone's resistance to loading (e.g., cross-sectional area, second moments of area; Biewener, 1992; Currey, 2002; Wainwright et al., 1976), and the three-dimensional architecture of cancellous bone in the epiphyses is strongly linked to the pattern of joint loading experienced in vivo (Bishop et al., 2018; Kivell, 2016; Pontzer et al., 2006). These aspects could vary significantly and not be detectable from external dimensions alone. Inclusion of internal geometry data could lead to an enriched, more nuanced assessment, yet obtaining a comprehensive dataset across the broad suite of taxa considered here would be a very large and expensive undertaking, requiring x-ray computed tomographic scanning or destructive physical sectioning. This is clearly not practical for many of the taxa studied here, and indeed, first-hand experience with the former method indicates that insufficient contrast between bone and matrix infill (necessary for the resolution of internal geometry) may sometimes not be attainable in many Permian-aged fossil specimens, without advanced scanning techniques such as phase-contrast synchrotron tomography (e.g., Benoit et al., 2024; Sanchez et al., 2013).

4.6.2 | Sampling

Although the present study provides the most comprehensive survey of stylopod evolution in non-therian synapsids to date, it is nevertheless limited by the practicalities of sampling an incomplete fossil record. In several parts of synapsid phylogeny, it was not possible to measure the earlier-diverging members of a given clade, which becomes critical when said taxa are smaller than their later-diverging relatives. For example, smaller, earlier-diverging anteosaurids (Dinocephalia), gorgonopsians, and non-dicynodont anomodonts are veritably absent from the study, as they are thus far inadequately represented by postcranial remains (e.g., Kammerer, 2011; Kammerer & Masyutin, 2018; Liu et al., 2010; Rubidge & Hopson, 1996). This may have important consequences for interpretations of the evolution of body size, wherein the true pattern is more subdued compared to the pattern recovered here (Figure 9d), at least for certain nodes on the therian stem lineage. Furthermore, analysis of most of the metrics examined here involves accounting for body size, and inadequate sampling of smaller, earlier-diverging taxa may bias ASRs of these metrics. This may explain the current results for certain diaphyseal dimensions, wherein basal therapsids are reconstructed as more robust than advanced "pelycosaurs" (Figure 5d,e,g). A similar scenario possibly explains basal mammals being reconstructed as more robust than advanced non-mammalian cynodonts (Figure 5c,e,g), with the fossorial monotremes (extant) and *Haldanodon* (extinct mammaliaform) biasing reconstructions for the Mammalia node. Sampling limitation may also produce the opposite effect, as in the case of less robust humeral dimensions at Mammaliaformes compared to preceding or succeeding nodes on the stem lineage (Figure 6). Rather than indicative of a transient trend reversal, this may be a symptom of limited sampling, wherein morganucodontids are anomalously gracile and most other early mammaliaform postcranial remains are presently too poorly preserved for reliable three-dimensional measurement.

A second sampling-related issue pertains to the preponderance of nodes in the cynodont part of the stem lineage which are subtended by individual species, rather than multi-species clades (Figure 1). ASRs at these particular nodes will be more influenced by variation in the traits exhibited by the adjoining species, since variation among the members of larger clades tends to be smoothed out. Reconstructed patterns of evolution will hence be more sensitive to variation among individual taxa, resulting from, for instance, ecological diversification. The node-to-node jitter often observed in reconstructions for the cynodont part of the stem lineage (cf. Figures 5–9) is likely attributable, at least in part, to this "singleton taxon" effect.

5 | CONCLUSION

An extensive survey of external dimensions of synapsid humeri and femora has provided the opportunity to address several important changes in locomotor biomechanics inferred to have taken place on the line to therian mammals. Exploring the evolution of bone proportions along the therian stem lineage has necessitated the development of a new method that accounts for the effect of size at the level of individual species. The underlying logic of this approach can be extended to a wide range of traits beyond bone proportions, including those expected to scale with length at exponents very different from one (e.g., areas, volumes, moments of inertia, etc.). The approach employed by the present study therefore provides a novel framework for investigating other major functional transitions in vertebrate evolution through the lens of individual bone morphology.

Evolutionary transformation of humeral and femoral proportions is broadly consistent with many functional

changes inferred to have taken place between basal synapsids and crown therians. Nevertheless, the pattern of transformation between these two endpoints can scarcely be regarded as linear. Broad patterns of change from basal synapsids to crown therians are frequently overprinted by nuances or trend reversals in various parts of synapsid phylogeny, especially within non-mammalian cynodonts and dicynodont anomodonts (cf. Bishop & Pierce, 2024c; Brocklehurst et al., 2025; Lungmus & Angielczyk, 2021), potentially indicating greater ecological specialization and diversification within these groups. In addition, stylopod proportions that typify therians as a whole are frequently not achieved until crown Theria itself. These results further paint a complex history of functional evolution in the synapsid fore- and hindlimb, with different clades or grades exploring different "styles" of locomotor function on the line to mammals, and with a therian "style" of locomotor function appearing relatively late in synapsid evolution (Bishop & Pierce, 2024c; Brocklehurst et al., 2025; Jones et al., 2024; Lungmus & Angielczyk, 2021).

AUTHOR CONTRIBUTIONS

P. J. Bishop: Conceptualization; data curation; formal analysis; funding acquisition; investigation; methodology; project administration; resources; software; validation; visualization; writing – original draft; writing – review and editing. **S. E. Pierce:** Conceptualization; investigation; funding acquisition; validation; visualization; writing – review and editing; methodology; writing – original draft; formal analysis; software; supervision; data curation; resources; project administration.

ACKNOWLEDGMENTS

Much appreciation is extended to the museum curatorial and collections staff for access to specimens in their care; in alphabetical order they are K. Angielczyk, E. Biedron, C. Browning, J. Botha, E. Butler, C. Byrd, M. Day, J. Escobar, M. Ezcurra, H. Francischini, H. Fourie, A. Gishlick, R. González, C. Green, P. Holroyd, H. Janetzki, S. Jirah, S. Johnston, A. Kowalczyk, A. Krahl, M. Lowe, A. Martinelli, R. Masters, N. Mchunu, C. Mehling, A. Millhouse, M. Omura, P. Ortiz, F. Pinheiro, F. Pretto, O. Rauhut, B. Rubidge, W. Simpson, Z. Skosan, R. Stebbings, A. Stroup, H. Sues, I. Werneburg, and B. Zipfel. In addition, K. Schoenberger, C. Sidor, D. Rovinsky, H. Richards, and L. Weaver are thanked for providing measurements of additional specimens that were not examined in person. This study benefited from helpful discussions with M. Wright, R. Brocklehurst, E. Hunt, T. Simões, C. Kammerer, K. Angielczyk, M. Day, and B. Stuart. Past and present members of the Pierce Lab are also thanked for their support and feedback, especially M. Wright, R. Brocklehurst, and G. Guilhon for providing digital scans. The logistical assistance of T. Barbaro and J. Hughes is also gratefully acknowledged. Lastly, S. Heritage and A. Huttenlocker, and the associate editor B. Patel, are sincerely thanked for constructive and insightful critiques of earlier versions of the manuscript.

FUNDING INFORMATION

This work was financially supported by the United States National Science Foundation, grants DEB-1754459 and EAR-2122115, and the William F. Milton Fund, Harvard University.

CONFLICT OF INTEREST STATEMENT

The authors declare no conflict of interest.

DATA AVAILABILITY STATEMENT

All data relating to this study are provided in Supporting Information S1–S6 or are accessioned in registered museum collections (see Supporting Information S2). Digital scan data of fossil material generated in this study is accessioned with the corresponding museum collection or is available via MorphoSource (see Supporting Information S2).

ORCID

P. J. Bishop https://orcid.org/0000-0003-2702-0557
S. E. Pierce https://orcid.org/0000-0003-0717-1841

REFERENCES

Aamodt, A., Lund-Larsen, J., Eine, J., Andersen, E., Benum, P., & Schnell Husby, O. (1997). *In vivo* measurements show tensile axial strain in the proximal lateral aspect of the human femur. *Journal of Orthopaedic Research*, *15*, 927–931.

Abdala, F. (2007). Redescription of *Platycraniellus elegans* (Therapsida, Cynodontia) from the Lower Triassic of South Africa and the cladistic relationships of Eutheriodontia. *Palaeontology*, *50*, 591–618.

Abdala, F., Gaetano, L. C., Smith, R. M. H., & Rubidge, B. S. (2019). A new large cynodont from the Late Permian (Lopingian) of the south African Karoo Basin and its phylogenetic significance. *Zoological Journal of the Linnean Society*, *186*, 983–1005.

Alexander, R. M. (1989). *Dynamics of dinosaurs and other extinct giants*. Columbia University Press.

Alexander, R. M. (2006). *Principles of animal locomotion*. Princeton University Press.

Allen, V., Paxton, H., & Hutchinson, J. R. (2009). Variation in center of mass estimates for extant sauropsids and its importance for reconstructing inertial properties of extinct archosaurs. *The Anatomical Record*, *292*, 1442–1461.

Alroy, J., Marshall, C., & Miller, A. (2012). The Paleobiology database. https://paleobiodb.org/

Angielczyk, K. D., & Kammerer, C. F. (2018). Non-mammalian synapsids: The deep roots of the mammalian family tree. In F.

Zachos & R. J. Asher (Eds.), *Mammalian evolution, diversity and systematics* (pp. 117–198). De Gruyter.

Ashley-Ross, M. A. (1995). Patterns of hind limb motor output during walking in the salamander *Dicamptodon tenebrosus*, with comparisons to other tetrapods. *Journal of Comparative Physiology A: Neuroethology, Sensory, Neural, and Behavioral Physiology*, *177*, 273–285.

Bapst, D. W. (2012). Paleotree: An R package for paleontological and phylogenetic analyses of evolution. *Methods in Ecology and Evolution*, *3*, 803–807.

Barak, M. M. (2024). Cortical and trabecular bone modeling and implications for bone functional adaptation in the mammalian tibia. *Bioengineering*, *11*, 514.

Bates, K. T., Falkingham, P. L., Macaulay, S., Brassey, C. A., & Maidment, S. C. R. (2015). Downsizing a giant: re-evaluating *Dreadnoughtus* body mass. *Biology Letters*, *11*, 20150215.

Bates, K. T., Mannion, P. D., Falkingham, P. L., Brusatte, S. L., Hutchinson, J. R., Otero, A., Sellers, W. I., Sullivan, C., Stevens, K. A., & Allen, V. (2016). Temporal and phylogenetic evolution of the sauropod dinosaur body plan. *Royal Society Open Science*, *3*, 150636.

Beer, F. P., Johnston, E. R., Jr., DeWolf, J. T., & Mazurek, D. F. (2012). *Mechanics of materials* (6th ed.). McGraw-Hill.

Bendel, E.-M., Kammerer, C. F., Kardjilov, N., Fernandez, V., & Fröbisch, J. (2018). Cranial anatomy of the gorgonopsian *Cynariops robustus* based on CT-reconstruction. *PLoS One*, *13*, e0207367.

Benoit, J., Araujo, R., Lund, E. S., Bolton, A., Lafferty, T., Macungo, Z., & Fernandez, V. (2024). Early synapsids neurosensory diversity revealed by CT and synchrotron scanning. *The Anatomical Record*. https://doi.org/10.1002/ar.25445

Benson, R. B. J., Godoy, P., Bronzati, M., Butler, E., & Gearty, W. (2022). Reconstructed evolutionary patterns for crocodile-line archosaurs demonstrate impact of failure to log-transform body size data. *Communications Biology*, *5*, 171.

Berman, D. S. (2013). Diadectomorphs, amniotes or not? *New Mexico Museum of Natural History and Science Bulletin*, *60*, 22–35.

Bertram, J. E. A., & Biewener, A. A. (1988). Bone curvature: Sacrificing strength for load predictability? *Journal of Theoretical Biology*, *131*, 75–92.

Bertram, J. E. A., & Biewener, A. A. (1990). Differential scaling of the long bones in the terrestrial carnivora and other mammals. *Journal of Morphology*, *204*, 157–169.

Biewener, A. A. (1989). Scaling body support in mammals: Limb posture and muscle mechanics. *Science*, *245*, 45–48.

Biewener, A. A. (1991). Musculoskeletal design in relation to body size. *Journal of Biomechanics*, *24*, 19–29.

Biewener, A. A. (1992). Overview of structural mechanics. In A. A. Biewener (Ed.), *Biomechanics: Structures and systems – A practical approach* (pp. 1–20). Oxford University Press.

Biewener, A. A., Swartz, S. M., & Bertram, J. E. A. (1986). Bone modelling during growth: Dynamics strain equilibrium in the chick tibiotarsus. *Calcified Tissue International*, *39*, 390–395.

Biewener, A. A., & Taylor, C. R. (1986). Bone strain: A determinant of gait and speed? *Journal of Experimental Biology*, *123*, 383–400.

Bishop, P. J., Bates, B. T., Allen, V. R., Henderson, D. M., Randau, M., & Hutchinson, J. R. (2020). Relationships of mass properties and body proportions to locomotor habit in terrestrial Archosauria. *Paleobiology*, *46*, 550–569.

Bishop, P. J., Brocklehurst, R. J., & Pierce, S. E. (2023). Intelligent sampling of high-dimensional joint mobility space for analysis of articular function. *Methods in Ecology and Evolution*, *14*, 569–582.

Bishop, P. J., Cuff, A. R., & Hutchinson, J. R. (2021). How to build a dinosaur: Musculoskeletal modeling and simulation of locomotor biomechanics in extinct animals. *Paleobiology*, *47*, 1–38.

Bishop, P. J., Hocknull, S. A., Clemente, C. J., Hutchinson, J. R., Farke, A. A., Barrett, R. S., & Lloyd, D. G. (2018a). Cancellous bone architecture and theropod dinosaur locomotion. Part III – Inferring posture and locomotor biomechanics in extinct theropods, and its evolution on the line to birds. *PeerJ*, *6*, e5777.

Bishop, P. J., Hocknull, S. A., Clemente, C. J., Hutchinson, J. R., Farke, A. A., Beck, B. R., Barrett, R. S., & Lloyd, D. G. (2018b). Cancellous bone architecture and theropod dinosaur locomotion. Part I – An examination of cancellous bone architecture in the hindlimb bones of theropods. *PeerJ*, *6*, 5778.

Bishop, P. J., & Pierce, S. E. (2024a). The fossil record of appendicular muscle evolution in Synapsida on the line to mammals. Part I – Forelimb. *The Anatomical Record*, *307*, 1764–1825.

Bishop, P. J., & Pierce, S. E. (2024b). The fossil record of appendicular muscle evolution in Synapsida on the line to mammals. Part II – Hindlimb. *The Anatomical Record*, *307*, 1826–1896.

Bishop, P. J., & Pierce, S. E. (2024c). Late acquisition of erect hindlimb posture and function in the forerunners of therian mammals. *Science Advances*, *10*, adr2722.

Blob, R. W. (2000). Interspecific scaling of the hindlimb skeleton in lizards, crocodilians, felids and canids: Does limb bone shape correlate with limb posture? *Journal of Zoology*, *250*, 507–531.

Blob, R. W. (2001). Evolution of hindlimb posture in nonmammalian therapsids: Biomechanical tests of paleontological hypotheses. *Paleobiology*, *27*, 14–38.

Blob, R. W. (2006). Scaling of the hind limb skeleton in cynognathian cynodonts: Implications for ontogeny and the evolution of mammalian endothermy. In M. T. Carrano, T. J. Gaudin, R. W. Blob, & J. R. Wible (Eds.), *Amniote paleobiology: Perspectives on the evolution of mammals, birds, and reptiles* (pp. 410–431). University of Chicago Press.

Blob, R. W., & Biewener, A. A. (1999). *In vivo* locomotor strain in the hindlimb bones of *Alligator mississippiensis* and *Iguana iguana*: Implications for the evolution of limb bone safety factor and non-sprawling limb posture. *Journal of Experimental Biology*, *202*, 1023–1046.

Blob, R. W., & Biewener, A. A. (2001). Mechanics of limb bone loading during terrestrial locomotion in the green iguana (*Iguana iguana*) and American alligator (*Alligator mississippiensis*). *Journal of Experimental Biology*, *204*, 1099–1122.

Blob, R. W., Espinoza, N. R., Butcher, M. T., Lee, A. H., D'Amico, A. R., Baig, F., & Sheffield, K. M. (2014). Diversity of limb-bone safety factors for locomotion in terrestrial vertebrates: Evolution and mixed chains. *Integrative and Comparative Biology*, *54*, 1058–1071.

Boonstra, L. D. (1934). A contribution to the morphology of the Gorgonopsia. *Annals of the South African Museum*, *31*, 137–174.

Boonstra, L. D. (1967). An early stage in the evolution of the mammalian quadrupedal walking gait. *Annals of the South African Museum*, *50*, 27–42.

Botha, J., Abdala, F., & Smith, R. M. H. (2007). The oldest cynodont: New clues on the origin and early diversification of the Cynodontia. *Zoological Journal of the Linnean Society*, *149*, 477–492.

Brassey, C. A., Maidment, S. C. R., & Barrett, P. M. (2015). Body mass estimates of an exceptionally complete *stegosaurus* (Ornithischia: Thyreophora): Comparing volumetric and linear bivariate mass estimation methods. *Biology Letters*, *11*, 20140984.

Brassey, C. A., Margetts, L., Kitchener, A. C., Withers, P. C., Manning, P. L., & Sellers, W. I. (2013). Finite element modelling versus classic beam theory: Comparing methods for stress estimation in a morphologically diverse sample of vertebrate long bones. *Journal of the Royal Society Interface*, *10*, 20120823.

Brocklehurst, N. (2019). Morphological evolution in therocephalians breaks the hypercarnivore ratchet. *Proceedings of the Royal Society B: Biological Sciences*, *286*, 20190590.

Brocklehurst, N., & Brink, K. S. (2017). Selection towards larger body size in both herbivorous and carnivorous synapsids during the carboniferous. *Facets*, *2*, 68–84.

Brocklehurst, R. J., Fahn-Lai, P., Regnault, S., & Pierce, S. E. (2022). Musculoskeletal modeling of sprawling and parasagittal forelimbs provides insight into synapsid postural transition. *iScience*, *25*, 103578.

Brocklehurst, R. J., Mercado, M., Angielczyk, K. D., & Pierce, S. E. (2025). Adaptive landscapes unveil the complex evolutionary path to mammalian forelimb function and posture in mammals. *PLOS Biology*, *23*, e3003188.

Broili, F., & Schröder, J. (1935). Über die Skelettrests einers Gorgonopsiers aus den unteren Beaufort-Schichten. In *Sitzungsberichte der Mathematisch-Naturwissenchaftlichen Abteilung der Baierischen Akademie der Wissenschaften Zu München* (pp. 279–330). Die Akademie.

Brusatte, S. L., Benton, M. J., Ruta, M., & Lloyd, G. T. (2008). Superiority, competition, and opportunism in the evolutionary radiation of dinosaurs. *Science*, *321*, 1485–1488.

Buchner, H. H. F., Savelberg, H. H. C. M., Schamhardt, H. C., & Barneveld, A. (1997). Inertial properties of dutch warmblood horses. *Journal of Biomechanics*, *30*, 653–658.

Butcher, M. T., & Blob, R. W. (2008). Mechanics of limb bone loading during terrestrial locomotion in river cooter turtles (*Pseudemys concinna*). *Journal of Experimental Biology*, *211*, 1187–1202.

Butcher, M. T., Espinoza, N. R., Cirilo, S. R., & Blob, R. W. (2008). *In vivo* strains in the femur of river cooter turtles (*Pseudemys concinna*) during terrestrial locomotion: Tests of force-platform models of loading mechanics. *Journal of Experimental Biology*, *211*, 2397–2407.

Butcher, M. T., White, B. J., Hudzik, N. B., Gosnell, W. C., Parrish, J. H. A., & Blob, R. W. (2011). *In vivo* strains in the femur of the Virginia opossum (*Didelphis viginiana*) during terrestrial locomotion: Testing hypotheses of evolutionary shifts in mammalian bone loading and design. *Journal of Experimental Biology*, *214*, 2631–2640.

Campione, N. E., & Evans, D. C. (2012). A universal scaling relationship between body mass and proximal limb bone dimensions in quadrupedal terrestrial animals. *BMC Biology*, *10*, 60.

Carrano, M. T. (1998). Locomotion in non-avian dinosaurs: Integrating data from hindlimb kinematics, in vivo strains, and bone morphology. *Paleobiology*, *24*, 450–469.

Carrano, M. T., & Biewener, A. A. (1999). Experimental alteration of limb posture in the chicken (*Gallus gallus*) and its bearing on the use of birds as analogs for dinosaur locomotion. *Journal of Morphology*, *240*, 237–249.

Carrier, D. R. (1983). Postnatal ontogeny of the musculo-skeletal system in the black-tailed jack rabbit (*Lepus californicus*). *Journal of Zoology*, *201*, 27–55.

Carrier, D. R., & Leon, L. R. (1990). Skeletal growth and function in the California gull (*Larus californicus*). *Journal of Zoology*, *222*, 375–389.

Carter, D. R., & Beaupré, G. S. (2001). *Skeletal function and form: Mechanobiology of skeletal development, aging, and regeneration*. Cambridge University Press.

Chan, N. R. (2016). Phylogenetic variation in hind-limb bone scaling of flightless theropods. *Paleobiology*, *43*, 129–143.

Chen, M., & Wilson, G. P. (2015). A multivariate approach to infer locomotor modes in Mesozoic mammals. *Paleobiology*, *41*, 280–312.

Christiansen, P. (1999a). Long bone scaling and limb posture in non-avian theropods: Evidence for differential allometry. *Journal of Vertebrate Paleontology*, *19*, 666–680.

Christiansen, P. (1999b). Scaling of mammalian long bones: Small and large mammals compared. *Journal of Zoology*, *247*, 333–348.

Cieri, R. L., Dick, T. J. M., Irwin, R., Rumsey, D., & Clemente, C. J. (2021). The scaling of ground reaction forces and duty factor in monitor lizards: Implications for locomotion in sprawling tetrapods. *Biology Letters*, *17*, 20200612.

Cluver, M. A. (1978). The skeleton of the mammal-like reptile *Cistecephalus* with evidence for a fossorial mode of life. *Annals of the South African Museum*, *76*, 213–246.

Coatham, S. J., Sellers, W. I., & Püschel, T. A. (2021). Convex hull estimation of mammalian body segment parameters. *Royal Society Open Science*, *8*, 210836.

Colbert, E. H. (1948). The mammal-like reptile *Lycaenops*. *Bulletin of the American Museum of Natural History*, *89*, 353–404.

Copploe, J. V., Blob, R. W., Parrish, J. H. A., & Butcher, M. T. (2015). In vivo strains in the femur of the nine-banded armadillo (*Dasypus novemcinctus*). *Journal of Morphology*, *276*, 889–899.

Cox, C. B. (1972). A new digging dicynodont from the Upper Permian of Tanzania. In K. A. Joysey & T. S. Kemp (Eds.), *Studies in vertebrate evolution* (pp. 173–189). Oliver & Boyd.

Currey, J. D. (2002). *Bones: Structure and mechanics*. Princeton University Press.

Damiani, R., Modesto, S. P., Yates, A. M., & Neveling, J. (2003). Earliest evidence of cynodont burrowing. *Proceedings of the Royal Society of London. Series B: Biological Sciences*, *270*, 1747–1751.

De Oliveira, T. V., & Schultz, C. L. (2016). Functional morphology and biomechanics of the cynodont *Trucidocynodon riograndensis* from the Triassic of Southern Brazil: Pectoral girdle and forelimb. *Acta Palaeontologica Polonica*, *61*, 377–386.

Demes, B., Larson, S. G., Stern, J. T., Jr., Jungers, W. L., Biknevicius, A. R., & Schmitt, D. (1994). The kinetics of primate quadrupedalism: "Hindlimb drive" reconsidered. *Journal of Human Evolution*, *26*, 353–374.

Demes, B., Qin, Y.-X., Stern, J. T., Jr., Larson, S. G., & Rubin, C. T. (2001). Patterns of strain in the macaque tibia during functional

activity. *American Journal of Physical Anthropology*, *116*, 257–265.

Demes, B., Stern, J. T., Jr., Hausman, M. R., Larson, S. G., McLeod, K. J., & Rubin, C. T. (1998). Patterns of strain in the macaque ulna during functional activity. *American Journal of Physical Anthropology*, *106*, 87–100.

Dial, K. P., Shubin, N. H., & Brainerd, E. L. (2015). *Great transformations in vertebrate evolution*. University of Chicago Press.

Dick, T. J. M., & Clemente, C. J. (2016). How to build your dragon: Scaling of muscle architecture from the world's smallest to the world's largest monitor lizard. *Frontiers in Zoology*, *13*, 8.

Didier, G., & Laurin, M. (2021). Distributions of extinction times from fossil ages and tree topologies: The example of mid-Permian synapsid extinctions. *PeerJ*, *9*, e12577.

Doube, M., Felder, A. A., Chua, M. Y., Lodhia, K., Kłosowski, M. M., Hutchinson, J. R., & Shefelbine, S. J. (2018). Limb bone scaling in hopping macropods and quadrupedal artiodactyls. *Royal Society Open Science*, *5*, 180152.

Doube, M., Yen, S. C. W., Kłosowski, M. M., Farke, A. A., Hutchinson, J. R., & Shefelbine, S. J. (2012). Whole-bone scaling of the avian pelvic limb. *Journal of Anatomy*, *221*, 21–29.

Edwards, L. F. (1937). Morphology of the forelimb of the mole (*Scalopus aquaticus*, L.) in relation to its fossorial habits. *The Ohio Journal of Science*, *37*, 20–41.

Fernandez, V., Abdala, F., Carlson, K. J., Cook, D. C., Rubidge, B. S., Yates, A. M., & Tafforeau, P. (2013). Synchrotron reveals Early Triassic odd couple: Injured amphibian and aestivating therapsid share burrow. *PLoS One*, *8*, e64978.

Filippini, F. S., Abdala, F., & Cassini, G. H. (2022). Body mass estimation in Triassic cynodonts from Argentina based on limb variables. *Acta Palaeontologica Polonica*, *67*, 543–557.

Fourie, H., & Rubidge, B. S. (2007). The postcranial skeletal anatomy of the therocephalian *Regisaurus* (Therapsida: Regisauridae) and its utilization for biostratigraphic correlation. *Palaeontologia Africana*, *42*, 1–16.

Fourie, H., & Rubidge, B. S. (2009). The postcranial skeleton of the basal therocephalian *Glanosuchus macrops* (Scylacosauridae) and comparison of morphological and phylogenetic trends amongst the Theriodontia. *Palaeontologia Africana*, *44*, 27–39.

Fröbisch, J. (2006). Locomotion in derived dicynodonts (Synapsida, Anomodontia): A functional analysis of the pelvic girdle and hind limb of *Tetragoniaa njalilus*. *Canadian Journal of Earth Sciences*, *43*, 1297–1308.

Fröbisch, J., & Reisz, R. R. (2009). The Late Permian herbivore *Suminia* and the early evolution of arboreality in terrestrial vertebrate ecosystems. *Proceedings of the Royal Society B: Biological Sciences*, *276*, 3611–3618.

Frongia, G. N., Muzzeddu, M., Mereu, P., Leoni, G., Berlinguer, F., Zedda, M., Farina, V., Satta, V., Di Stefano, M., & Naitana, S. (2018). Structural features of cross-sectional wing bones in the griffon vulture (*Gyps fulvus*) as a prediction of flight style. *Journal of Morphology*, *279*, 1753–1763.

Fujiwara, S., & Hutchinson, J. R. (2012). Elbow joint adductor moment arm as an indicator of forelimb posture in extinct quadrupedal tetrapods. *Proceedings of the Royal Society of London. Series B*, *279*, 2561–2570.

Galilei, G. (1638). *Discorsi e dimostrazioni matematiche intorno à due nuoue scienze attenenti alla mecanica i movimenti locali*. Appresso gli Elsevirii.

Gambaryan, P. P., & Kielan-Jaworowska, Z. (1997). Sprawling *versus* parasagittal stance in multituberculate mammals. *Acta Palaeontologica Polonica*, *42*, 13–44.

Gambaryan, P. P., Kuznetsov, A. N., Panyutina, A. A., & Gerasimov, S. V. (2015). Shoulder girdle and forelimb myology of extant Monotremata. *Russian Journal of Theriology*, *14*, 1–56.

Gatesy, S. M. (1991). Hind limb scaling in birds and other theropods: Implications for terrestrial locomotion. *Journal of Morphology*, *209*, 83–96.

Gatesy, S. M. (1997). An electromyographic analysis of hindlimb function in *Alligator* during terrestrial locomotion. *Journal of Morphology*, *234*, 197–212.

Georgiou, L., Dunmore, C. J., Bardo, A., Buck, L. T., Hublin, J.-J., Pahr, D. H., Stratford, D., Synek, A., Kivell, T. L., & Skinner, M. M. (2020). Evidence for habitual climbing in a Pleistocene hominin in South Africa. *Proceedings of the National Academy of Sciences*, *117*, 8416–8423.

Goslow, G. E., Jr., Seeherman, H. J., Taylor, C. R., McCutchin, M. N., & Heglund, N. C. (1981). Electrical activity and relative length changes of dog limb muscles as a function of speed and gait. *Journal of Experimental Biology*, *94*, 15–42.

Govender, R. (2008). Description of the postcranial anatomy of *Aulacephalodon baini* and its possible relationship with '*Aulacephalodon peavoti*'. *South African Journal of Science*, *104*, 479–486.

Gregory, W. K. (1926). The skeleton of *Moschops capensis* broom, a dinocephalian reptile from the Permian of South Africa. *Bulletin of the American Museum of Natural History*, *61*, 179–251.

Griffin, C. T., & Angielczyk, K. D. (2019). The evolution of the dicynodont sacrum: Constraint and innovation in the synapsid axial column. *Paleobiology*, *45*, 201–220.

Groenewald, G. H., Welman, J., & MacEachern, J. A. (2001). Vertebrate burrow complexes from the Early Triassic Cynognathus zone (Driekoppen formation, Beaufort group) of the Karoo Basin, South Africa. *PALAIOS*, *16*, 148–160.

Guignard, M. L., Martinelli, A. G., & Soares, M. B. (2019). The postcranial anatomy of *Brasilodon quadrangularis* and the acquisition of mammaliaform traits among non-mammaliaform cynodonts. *PLoS One*, *14*, e0216672.

Hedges, S. B., Dudley, J., & Kumar, S. (2006). TimeTree: A public knowledge-base of divergence times among organisms. *Bioinformatics*, *22*, 2971–2972.

Hellert, S. M., Grossnickle, D. M., Lloyd, G. T., Kammerer, C. F., & Angielczyk, K. D. (2023). Derived faunivores are the forerunners of major synapsid radiations. *Nature Ecology & Evolution*, *7*, 1903–1913.

Holliday, C. M., Ridgely, R. C., Sedlmayr, J. C., & Witmer, L. M. (2010). Cartilaginous epiphyses in extant archosaurs and their implications for reconstructing limb function in dinosaurs. *PLoS One*, *5*, e13120.

Hopson, J. A. (2015). Fossils, trackways, and transitions in locomotion: A case study of *dimetrodon*. In K. P. Dial, N. H. Shubin, & E. L. Brainerd (Eds.), *Great transformations in vertebrate evolution*. University of Chicago Press.

Hutchinson, J. R., & Gatesy, S. M. (2000). Adductors, abductors, and the evolution of archosaur locomotion. *Paleobiology*, *26*, 734–751.

Huttenlocker, A. K. (2014). Body size reductions in nonmammalian eutheriodont therapsids (Synapsida) during the end-Permian mass extinction. *PLoS One*, *9*, e87553.

Huttenlocker, A. K., & Sidor, C. A. (2020). A basal nonmammaliaform cynodont from the Permian of Zambia and the origins of mammalian endocranial and postcranial anatomy. *Journal of Vertebrate Paleontology*, *40*, e1827413.

Huttenlocker, A. K., Singh, S. A., Henrici, A. C., & Sumida, S. S. (2021). A carboniferous synapsid with caniniform teeth and a reappraisal of mandibular size-shape heterodonty in the origin of mammals. *Royal Society Open Science*, *8*, 211237.

Huttenlocker, A. K., & Smith, R. M. H. (2017). New whaitsioids (Therapsida: Therocephalia) from the Teekloof formation of South Africa and therocephalian diversity during the end-Guadalupian extinction. *PeerJ*, *5*, e3868.

Jenkins, F. A., Jr., & Goslow, G. E., Jr. (1983). The functional anatomy of the shoulder of the Savannah monitor lizard (*Varanus exanthematicus*). *Journal of Morphology*, *175*, 195–216.

Jenkins, F. A., Jr., & Parrington, F. R. (1976). The postcranial skeletons of the Triassic mammals *Eozostrodon*, *Megazostrodon* and *Erythrotherium*. *Philosophical Transactions of the Royal Society of London. Series B: Biological Sciences*, *273*, 387–431.

Jenkins, F. A., Jr., & Weijs, W. A. (1979). The functional anatomy of the shoulder in the Virginia opossum (*Didelphis virginiana*). *Journal of Zoology*, *188*, 379–410.

Jenkins, F. A., Jr. (1971a). Limb posture and locomotion in the Virginia opossum (*Didelphis virginiana*) and in other non-cursorial mammals. *Journal of Zoology*, *165*, 303–315.

Jenkins, F. A., Jr. (1971b). The postcranial skeleton of African cynodonts. *Bulletin of the Peabody Museum of Natural History*, *36*, 1–216.

Jenkins, F. A., Jr. (1973). The functional anatomy and evolution of the mammalian Humero-ulnar articulation. *American Journal of Anatomy*, *137*, 281–298.

Jones, K. E., Angielczyk, K. D., & Pierce, S. E. (2024). Origins of mammalian vertebral function revealed through digital bending experiments. *Proceedings of the Royal Society B: Biological Sciences*, *291*, 20240820.

Jones, K. E., Angielczyk, K. D., Polly, P. D., Head, J. J., Fernandez, V., Lungmus, J. K., Tulga, S., & Pierce, S. E. (2018). Fossils reveal the complex evolutionary history of the mammalian regionalized spine. *Science*, *361*, 1249–1252.

Jones, K. E., Dickson, B. V., Angielczyk, K. D., & Pierce, S. E. (2021). Adaptive landscapes challenge "lateral-to-sagittal" paradigm for mammalian vertebral evolution. *Current Biology*, *31*, 1883–1892.

Jones, K. E., Gonzalez, S., Angielczyk, K. D., & Pierce, S. E. (2020). Regionalization of the axial skeleton predates functional adaptation in the forerunners of mammals. *Nature Ecology & Evolution*, *4*, 470–478.

Kaiuca, J. F. L., Martinelli, A. G., Schultz, C. L., Fonseca, P. H. M., Taveres, W. C., & Soares, M. B. (2024). Weighing in on miniaturization: New body mass estimates for Triassic eucynodonts and analyses of body size evolution during the cynodont-mammal transition. *The Anatomical Record*, *307*, 1594–1612.

Kammerer, C. F. (2011). Systematics of the Anteosauria (Therapsida: Dinocephalia). *Journal of Systematic Palaeontology*, *9*, 261–304.

Kammerer, C. F. (2016). Systematics of the Rubidgeinae (Therapsida: Gorgonopsia). *PeerJ*, *4*, e1608.

Kammerer, C. F. (2023). Revision of the Scylacosauridae (Therapsida: Therocephalia). *Palaeontologia Africana*, *56*, 51–87.

Kammerer, C. F., & Masyutin, V. (2018). Gorgonopsian therapsids (*Nochnitsa* gen. Nov. and *Viatkogorgon*) from the Permian Kotelnich locality of Russia. *PeerJ*, *6*, e4954.

Kammerer, C. F., & Ordoñez, M. A. (2021). Dicynodonts (Therapsida: Anomodontia) of South America. *Journal of South American Earth Sciences*, *108*, 103171.

Keller, T. S., & Spengler, D. M. (1989). Regulation of bone stress and strain in the immature and mature rat femur. *Journal of Biomechanics*, *22*, 1115–1127.

Kemp, T. S. (1978). Stance and gait in the hindlimb of a therocephalian mammal-like reptile. *Journal of Zoology*, *186*, 143–161.

Kemp, T. S. (1980a). Aspects of the structure and functional anatomy of the Middle Triassic cynodont *Luangwa*. *Journal of Zoology*, *191*, 193–239.

Kemp, T. S. (1980b). The primitive cynodont *Procynosuchus*: Structure, function and evolution of the postcranial skeleton. *Philosophical Transactions of the Royal Society of London, Series B: Biological Sciences*, *288*, 217–258.

Kemp, T. S. (1982). *Mammal-like reptiles and the origin of mammals*. Academic Press.

Kemp, T. S. (1986). The skeleton of a baurioid therocephalian therapsid from the Lower Triassic (*Lystrosaurus* zone) of South Africa. *Journal of Vertebrate Paleontology*, *6*, 215–232.

Kemp, T. S. (2005). *The origin and evolution of mammals*. Oxford University Press.

Kemp, T. S. (2016). *The origin of higher taxa*. Oxford University Press.

Kerber, L., Martinelli, A. G., Müller, R. T., & Pretto, F. A. (2022). A new specimen provides insight into the anatomy of *Irajatherium hernandezi*, a poorly known probainognathian cynodont from the Late Triassic of southern Brazil. *The Anatomical Record*, *305*, 3113–3132.

King, G. M. (1981). The functional anatomy of a Permian dicynodont. *Philosophical Transactions of the Royal Society of London, Series B: Biological Sciences*, *291*, 243–322.

King, G. M. (1985). The postcranial skeleton of *Kingoria nowacki* (von Huene) (Therapsida: Dicynodontia). *Zoological Journal of the Linnean Society*, *84*, 263–289.

King, G. M. (1988). Anomodontia. *Handbuch der Paläoherpetologie Part 17C*, 1–171.

King, G. M. (1990). *The dicynodonts: A study in palaeobiology*. Chapman and Hall.

Kivell, T. L. (2016). A review of trabecular bone functional adaptation: What have we learned from trabecular analyses in extant hominoids and what can we apply to fossils? *Journal of Anatomy*, *228*, 569–594.

Kozłowski, J., & Wiener, J. (1997). Interspecific allometries are by-products of body size optimization. *The American Naturalist*, *149*, 352–380.

Labonte, D., Clemente, C. J., Dittrich, A., Kuo, C.-Y., Crosby, A. J., Irschick, D. J., & Federle, W. (2016). Extreme positive allometry of animal adhesive pads and the size limits of adhesion-based climbing. *Proceedings of the National Academy of Sciences*, *113*, 1297–1302.

Lai, P. H., Biewener, A. A., & Pierce, S. E. (2018). Three-dimensional mobility and muscle attachments in the pectoral limb of the Triassic cynodont *Massetognathus pascuali* (Romer, 1967). *Journal of Anatomy*, *232*, 383–406.

Lieberman, D. E., Polk, J. D., & Demes, B. (2004). Predicting long bone loading from cross-sectional geometry. *American Journal of Physical Anthropology*, *123*, 156–171.

Liu, J., Rubidge, B. S., & Li, J. (2010). A new specimen of *Biseridens qilianicus* indicates its phylogenetic position as the most basal anomodont. *Proceedings of the Royal Society B: Biological Sciences*, *277*, 285–292.

Lovejoy, C. O., Meindl, R. S., Ohman, J. C., Heiple, K. G., & White, T. D. (2002). The Maka femur and its bearing on the antiquity of human walking: Applying contemporary concepts of morphogenesis to the human fossil record. *American Journal of Physical Anthropology*, *119*, 97–133.

Lungmus, J. K., & Angielczyk, K. D. (2019). Antiquity of forelimb ecomorphological diversity in the mammalian stem lineage (Synapsida). *Proceedings of the National Academy of Sciences*, *116*, 6903–6907.

Lungmus, J. K., & Angielczyk, K. D. (2021). Phylogeny, function and ecology in the deep evolutionary history of the mammalian forelimb. *Proceedings of the Royal Society B: Biological Sciences*, *288*, 20210494.

Macaulay, S., Hoehfurtner, T., Cross, S. R. R., Marek, R. D., Hutchinson, J. R., Schachner, E. R., Maher, A. E., & Bates, K. T. (2023). Decoupling body shape and mass distribution in birds and their dinosaurian ancestors. *Nature Communications*, *14*, 1575.

Maidment, S. C. R., Linton, D. H., Upchurch, P., & Barrett, P. M. (2012). Limb-bone scaling indicates diverse stance and gait in quadrupedal ornithischian dinosaurs. *PLoS One*, *7*, e36904.

Main, R. P., & Biewener, A. A. (2004). Ontogenetic patterns of limb loading, *in vivo* bone strains and growth in the goat radius. *Journal of Experimental Biology*, *207*, 2577–2588.

Main, R. P., & Biewener, A. A. (2007). Skeletal strain patterns and growth in the emu hindlimb during ontogeny. *Journal of Experimental Biology*, *210*, 2676–2690.

Main, R. P., Simons, E. L. R., & Lee, A. H. (2021). Interpreting mechanical function in extant and fossil long bones. In V. de Buffrénil, A. J. de Ricqlès, L. Zylberberg, & K. Padian (Eds.), *Vertebrate skeletal histology and paleohistology* (pp. 688–723). CRC Press.

Marquez-Florez, K., Arroyave-Tobon, S., Tadrist, L., & Linares, J.-M. (2024). Elbow dimensions in quadrupedal mammals driven by lubrication regime. *Scientific Reports*, *14*, 2177.

Martin, R. B., Burr, D. B., & Sharkey, N. A. (1998). *Skeletal tissue mechanics*. Springer.

McPhee, B. W., Benson, R. B. J., Botha-Brink, J., Bordy, E. M., & Choiniere, J. N. (2018). A giant dinosaur from the earliest Jurassic of South Africa and the transition to quadrupedality in early sauropodomorphs. *Current Biology*, *28*, 3143–3151.

Molnar, J. L. (2021). Variation in articular cartilage thickness among extant salamanders and implications for limb function in stem tetrapods. *Frontiers in Ecology and Evolution*, *9*, 671006.

Morato, L., Schultz, C. L., Vega-Dias, C., Da Silva, F. P., & Kindlein, W. (2008). Discussing a myth: Biomechanical comparisons between *Dinodontosaurus* (Synapsida, Dicynodontia) and extinct ground sloths. *Arquivos Do Museu Nacional Do Rio de Janeiro*, *66*, 145–154.

Nakai, D., & Fujiwara, S. (2023). Fossorial mammals emphasise the forelimb muscle moment arms used for digging: New indices for reconstruction of the digging ability and behaviours in extinct taxa. *Journal of Anatomy*, *242*, 846–861.

Nicolopoulos-Stournaras, S., & Iles, J. F. (1984). Hindlimb muscle activity during locomotion in the rat (*Rattus norvegicus*) (Rodentia: Muridae). *Journal of Zoology*, *203*, 427–440.

Orme, D., Freckleton, R., Thomas, G., Petzoldt, T., Fritz, S., Isaac, N., & Pearse, W. (2018). caper: Comparative analyses of phylogenetics and evolution in R. https://CRAN.R-project.org/package=caper

Pandy, M. G., Kumar, V., Berme, N., & Waldron, K. J. (1988). The dynamics of quadrupedal locomotion. *Journal of Biomechanical Engineering*, *110*, 230–237.

Paradis, E., & Schliep, K. (2019). Ape 5.0: An environment for modern phylogenetics and evolutionary analysis in R. *Bioinformatics*, *35*, 526–528.

Pearson, O. M., & Lieberman, D. E. (2004). The aging of Wolff's "law": Ontogeny and responses to mechanical loading in cortical bone. *Yearbook of Physical Anthropology*, *47*, 63–99.

Pierce, S. E., Lamas, L. P., Pelligand, L., Schilling, N., & Hutchinson, J. R. (2020). Patterns of limb and epaxial muscle activity during walking in the fire salamander, *Salamandra salamandra*. *Integrative Organismal Biology*, *2*, obaa015.

Pintore, R., Houssaye, A., Nesbitt, S. J., & Hutchinson, J. R. (2022). Femoral specializations to locomotor habits in early archosauriforms. *Journal of Anatomy*, *240*, 867–892.

Pintore, R., Hutchinson, J. R., Bishop, P. J., Tsai, H. P., & Houssaye, A. (2024). The evolution of femoral morphology in giant non-avian theropod dinosaurs. *Paleobiology*, *50*, 308–329.

Polly, P. D. (2007). Limbs in mammalian evolution. In B. K. Hall (Ed.), *Fins into limbs: Evolution, development, and transformation*. University of Chicago Press.

Pontzer, H., Lieberman, D. E., Momin, E., Devlin, M. J., Polk, J. D., Hallgrímsson, B., & Cooper, D. M. L. (2006). Trabecular bone in the bird knee responds with high sensitivity to changes in load orientation. *Journal of Experimental Biology*, *209*, 57–65.

Pravoslavev, P. A. (1927). *Gorgonopsidae from the North Dwina excavations of V.P. Amalitzki*. U.S.S.R. Academy of Sciences.

Pusch, L. C., Kammerer, C. F., & Fröbisch, J. (2024). The origin and evolution of Cynodontia (Synapsida, Therapsida): Reassessment of the phylogeny and systematics of the earliest members of this clade using 3D-imaging technologies. *The Anatomical Record*, *307*, 1634–1730.

R Core Team. (2021). *R: A language and environment for statistical computing*. R Foundation for Statistical Computing.

Ramanujan, S. (1914). Modular equations and approximations to π. *Quarterly Journal of Mathematics*, *45*, 350–372.

Ray, S. (2006). Functional and evolutionary aspects of the postcranial anatomy of dicynodonts (Synapsida, Therapsida). *Palaeontology*, *49*, 1263–1286.

Ray, S., & Chinsamy, A. (2003). Functional aspects of the postcranial anatomy of the Permian dicynodont *Diictodon* and their ecological implications. *Palaeontology*, *46*, 151–183.

Regnault, S., Fahn-Lai, P., & Pierce, S. E. (2021). Validation of an echidna forelimb musculoskeletal model using XROMM and diceCT. *Frontiers in Bioengineering and Biotechnology*, *9*, 751518.

Reilly, S. M. (1995). Quantitative electromyography and muscle function of the hind limb during quadrupedal running in the lizard *Sceloporus clarki*. *Zoology*, *98*, 263–277.

Reisz, R. R. (1972). Pelycosaurian reptiles from the middle Pennsylvanian of North America. *Bulletin of the Museum of Comparative Zoology*, *144*, 27–62.

Ren, L., Miller, C. E., Lair, R., & Hutchinson, J. R. (2010). Integration of biomechanical compliance, leverage, and power in elephant limbs. *Proceedings of the National Academy of Sciences*, *107*, 7078–7082.

Revell, L. J. (2024). Phytools 2.0: An updated R ecosystem for phylogenetic comparative methods (and other things). *PeerJ*, *12*, e16505.

Rewcastle, S. C. (1980). Form and function in lacertilian knee and mesotarsal joints; a contribution to the analysis of sprawling locomotion. *Journal of Zoology*, *191*, 147–170.

Rewcastle, S. C. (1983). Fundamental adaptations in the lacertilian hind limb: A partial analysis of the sprawling limb posture and gait. *Copeia*, *1983*, 476–487.

Richards, H. L., Wells, R. T., Evans, A. R., Fitzgerald, E. M. G., & Adams, J. W. (2019). The extraordinary osteology and functional morphology of the limbs in Palorchestidae, a family of strange extinct marsupial giants. *PLoS One*, *14*, e0221824.

Romano, M. (2017). Long bone scaling of caseid synapsids: A combined morphometric and cladistic approach. *Lethaia*, *50*, 511–526.

Romano, M., & Manucci, F. (2021). Resizing *Lisowicia bojani*: Volumetric body mass estimate and 3D reconstruction of the giant Late Triassic dicynodont. *Historical Biology*, *33*, 474–479.

Romano, M., Manucci, F., Rubidge, B. S., & Van den Brandt, M. J. (2021). Volumetric body mass estimate and *in vivo* reconstruction of the Russian Pareiasaur *Scutosaurus karpinskii*. *Frontiers in Ecology and Evolution*, *9*, 692035.

Romano, M., & Rubidge, B. S. (2021). First 3D reconstruction and volumetric body mass estimate of the tapinocephalid dinocephalian *Tapinocaninus pamelae* (Synapsida: Therapsida). *Historical Biology*, *33*, 498–505.

Romer, A. S. (1922). The locomotor apparatus of certain primitive and mammal-like reptiles. *Bulletin of the American Museum of Natural History*, *46*, 517–606.

Romer, A. S., & Price, L. I. (1940). Review of the Pelycosauria. *Special Papers of the Geological Society of America*, *28*, 1–538.

Rubidge, B. S., & Hopson, J. A. (1996). A primitive anomodont therapsid from the base of the Beaufort group (Upper Permian) of South Africa. *Zoological Journal of the Linnean Society*, *117*, 115–139.

Rubidge, B. S., King, G. M., & Hancock, J. A. (1994). The postcranial skeleton of the earliest dicynodont synapsid *Eodicynodon* from the Upper Permian of South Africa. *Palaeontology*, *37*, 397–408.

Samuels, J. X., Meachen, J. A., & Sakai, S. A. (2013). Postcranial morphology and the locomotor habits of living and extinct carnivorans. *Journal of Morphology*, *274*, 121–146.

Sanchez, S., Fernandez, V., Pierce, S. E., & Tafforeau, P. (2013). Homogenization of sample absorption for the imaging of large and dense fossils with synchrotron microtomography. *Nature Protocols*, *8*, 1708–1717.

Sargis, E. J. (2002). Functional morphology of the hindlimb of tupaiids (Mammalia, Scandentia) and its phylogenetic implications. *Journal of Morphology*, *254*, 149–185.

Schmidt-Nielsen, K. (1985). *Scaling: Why is animal size so important?* Cambridge University Press.

Sereno, P. C. (2006). Shoulder girdle and forelimb in multituberculates: Evolution of parasagittal forelimb posture in mammals. In M. T. Carrano, T. J. Gaudin, R. W. Blob, & J. R. Wible (Eds.), *Amniote paleobiology: Perspectives on the evolution of mammals, birds, and reptiles* (pp. 315–366). University of Chicago Press.

Sheffield, K. M., & Blob, R. W. (2011). Loading mechanics of the femur in tiger salamanders (*Ambystoma tigrinum*) during terrestrial locomotion. *Journal of Experimental Biology*, *214*, 2603–2615.

Sheffield, K. M., Butcher, M. T., Shugart, S. K., Gander, J. C., & Blob, R. W. (2011). Locomotor loading mechanics in the hindlimbs of tegu lizards (*Tupinambis merianae*): Comparative and evolutionary implications. *Journal of Experimental Biology*, *214*, 2603–2615.

Sidor, C. A., Kulik, Z. T., & Huttenlocker, A. K. (2021). A new bauriamorph therocephalian adds a novel component to the Lower Triassic tetrapod assemblage of the Fremouw formation (Transantarctic Basin) of Antarctica. *Journal of Vertebrate Paleontology*, *41*, e2081510.

Sigogneau, D. (1970). *Révision systématique des Gorgonopsiens sud-africains*. Centre National de la Recherche Scientifique.

Simões, T. R., Kammerer, C. F., Caldwell, M. W., & Pierce, S. E. (2022). Successive climate crises in the deep past drove the early evolution and radiation of reptiles. *Science Advances*, *8*, eabq1898.

Singh, S. A., Elsler, A., Stubbs, T. L., Rayfield, E. J., & Benton, M. J. (2024). Predatory synapsid ecomorphology signals growing dynamism of Late Palaeozoic terrestrial ecosystems. *Communications Biology*, *7*, 201.

Smith-Paredes, D., Vergara-Cereghino, M. E., Lord, A., Moses, M. M., Behringer, R. R., & Bhullar, B.-A. S. (2022). Embryonic muscle splitting patterns reveal homologies of amniote forelimb muscles. *Nature Ecology & Evolution*, *6*, 604–613.

Spence, A. J. (2009). Scaling in biology. *Current Biology*, *19*, R57–R61.

Sullivan, C., Liu, J., Roberts, E. M., Huang, T. D., Yang, C., & Zhong, S. (2013). Pelvic morphology of a tritylodontid (Synapsida: Eucynodontia) from the Lower Jurassic of China, and some functional and phylogenetic implications. *Comptes Rendus Palevol*, *12*, 505–518.

Sumida, S. S. (1997). Locomotor features of taxa spanning the origin of amniotes. In S. S. Sumida & K. L. M. Martin (Eds.), *Amniote origins: Completing the transition to land* (pp. 353–398). Academic Press.

Swartz, S. M., & Biewener, A. A. (1992). Shape and scaling. In A. A. Biewener (Ed.), *Biomechanics – Structures and systems: A practical approach*. Oxford University Press.

Szivek, J. A., Johnson, E. M., & Magee, F. P. (1992). In vivo strain analysis of the greyhound femoral diaphysis. *Journal of Investigative Surgery*, *5*, 91–108.

Tatarinov, L. P. (2004). A postcranial skeleton of the Gorgonopian *Viatkogorgon ivachnenkoi* (Reptilia, Theriodontia) from the Upper Permian Kotelnich locality, Kirov region. *Paleontological Journal*, *38*, 437–447.

Taylor, G. K., & Thomas, A. L. R. (2014). *Evolutionary biomechanics – selection, phylogeny, and constraint*. Oxford University Press.

Thomason, J. J. (1985). The relationship of trabecular architecture to inferred loading patterns in the third metacarpals of the

extinct equids *Merychippus* and *Mesohippus*. *Paleobiology*, *11*, 323–335.

Tsai, H. P., & Holliday, C. M. (2015). Articular soft tissue anatomy of the archosaur hip joint: Structural homology and functional implications. *Journal of Morphology*, *276*, 601–630.

Van Valkenburgh, B. (1987). Skeletal indicators of locomotor behaviour in living and extinct carnivores. *Journal of Vertebrate Paleontology*, *7*, 162–182.

Venditti, C., Baker, J., & Barton, R. A. (2024). Co-evolutionary dynamics of mammalian brain and body size. *Nature Ecology & Evolution*, *8*, 1534–1542. https://doi.org/10.1038/s41559-41024-02451-41553

Vogel, S. (2003). *Comparative biomechanics: Life's physical world*. Princeton University Press.

von Huene, F. (1950). Die Theriodontier des ostafrikanischen Ruhuhu-Gebietes in der Tübinger Sammlung. *Neus Jahrbuch für Geologie und Palaontologie*, *92*, 47–136.

Wainwright, S. A., Biggs, W. D., Currey, J. D., & Gosline, J. M. (1976). *Mechanical design in organisms*. Edward Arnold (Publishers) Limited.

Wallace, I. J., Demes, B., M, C., Pearson, O. M., Polk, J. D., & Lieberman, D. E. (2014). Exercise-induced bone formation is poorly linked to local strain magnitude in the sheep tibia. *PLoS One*, *9*, e99108.

Warburton, N. M. (2006). Functional morphology of marsupial moles (Marsupialia, Notoryctidae). *Verhandlungen des Naturwissenschaftlichen Vereins in Hamburg*, *42*, 39–149.

Watson, D. M. S. (1917). The evolution of the tetrapod shoulder girdle and fore-limb. *Journal of Anatomy*, *52*, 1–63.

Watson, D. M. S. (1931). On the skeleton of a bauriamorph reptile. *Proceedings of the Zoological Society of London*, *101*, 1163–1205.

Willey, J. S., Biknevicius, A. R., Reilly, S. M., & Earls, K. D. (2004). The tale of the tail: Limb function and locomotor mechanics in *Alligator mississipiensis*. *Journal of Experimental Biology*, *207*, 553–563.

Witte, T. H., Knill, K., & Wilson, A. M. (2004). Determination of peak vertical ground reaction force from duty factor in the horse (*Equus caballus*). *Journal of Experimental Biology*, *207*, 3639–3648.

Wright, M. A., Cavanaugh, T. J., & Pierce, S. E. (2024). Evaluating the accuracy and precision of volumetric versus element-scaling body mass estimation. *Integrative Organismal Biology*, *6*, obae034.

Young, V. K. H., Vest, K. G., Rivera, A. R. V., Espinoza, N. R., & Blob, R. W. (2017). One foot out the door: Limb function during swimming in terrestrial versus aquatic turtles. *Biology Letters*, *13*, 20160732.

SUPPORTING INFORMATION

Additional supporting information can be found online in the Supporting Information section at the end of this article.

How to cite this article: Bishop, P. J., & Pierce, S. E. (2025). Locomotor shifts, stylopod proportions, and the evolution of allometry in Synapsida. *The Anatomical Record*, 1–31. https://doi.org/10.1002/ar.70006